Politecnico di Torino

Master's Degree in Biomedical Engineering

Master's Degree Thesis

Development of a biomimetic alveolus-on-chip to model the physiological alveolar barrier by supporting multicellular culture and air-liquid interface implementation.

Supervisors:
Prof. Matteo Cocuzza
Prof. Gianluca Ciardelli
Prof. Chiara Tonda-Turo

Candidate:
Maria Giovanna De Pasquale

Academic year 2022/2023

Ai miei genitori,
Fortunato e Manuela

Contents

List of plots

Abstract

The respiratory system is exposed to harmful substances reaching the lung during the breathing cycle. For this reason, studying the role of alveolar-capillary barrier in the pulmonary homeostasis plays a fundamental role to understand the pathophysiology of diseases associated with this barrier, such as the asthma, Idiopathic pulmonary fibrosis (IPF), Chronic obstructive pulmonary disease (COPD) and Coronavirus disease 2019 (COVID-19). To achieve this purpose, engineering microdevices platforms called Organ-on-chips (OoCs) are implemented to study the mechanism underlying the functions of a tissue, analyzing the cells environment and fluidic behavior. OoCs are high-throughput in vitro models that describe the architecture, the functionality and dynamic physiological environment into a miniaturized scale in order to analyze in vivo pathological conditions.

The objective of this Master thesis work is the development of an alveolus-on-chip system to mimic the alveolar barrier. The main goal is focused to recreate in vitro the thickest portion of the alveolar barrier, characterized by the presence of a collagen hydrogel, and the implementation of the air-liquid interface (ALI) in the apical compartment of the device to mimic the natural environment inside the alveolus. The system comprises a microfluidic platform made of polydimethylsiloxane (PDMS), which incorporates a nanofibrous PCL/Gelatin membrane (80:20) obtained by electrospinning to mimic the basement membrane of the alveolar barrier and a type I collagen hydrogel loading fibroblasts to reproduce the stromal tissue.

The starting point for the development of this work is the optimization of a functional geometry of the PDMS device. The PDMS layers constituting the alveolus-on-chip are obtained from poly(methyl methacrylate) (PMMA) molds, designed through Rhinoceros software and produced by laser ablation technique with a Poly-Jet 3D printer. In order to ensure the ALI and to reduce the tendence of liquid to flow back towards the inlet and/or to rise above the nanofibrous PCL/Gelatin membrane, the two microfluidic channels are connected to valvular conduits designed on a Nikola Tesla's original patent that are tested with colored water via microscope comparing the final device with and without valvular conduits. A co-culture was set within the here design OoC by pouring collagen based hydrogel loading MRC-5 fibroblasts above the electrospun membrane and then seeding A549 epithelial cells atop.

The resulting model is characterized at different time pointing through fluorescence imaging (DAPI, to perform the staining of the nuclei, and Phalloidin, to evaluate the staining of the actin filaments). The images show that the adopted multi-culture protocol allows the epithelial cells as well as fibroblasts inside the hydrogel to reach confluence with close cell-cell contact and a spread morphology, respectively. In addition, immunostaining tests were conducted to assess the barrier function of the model. These tests demonstrate the confluence of epithelial cells, which is determined by detecting the expression of E-cadherin (epithelial cadherin), and the enhanced proliferation of fibroblasts inside the bioinspired collagen hydrogel through the detection of Vimentin ex-

pression. Moreover, live/dead staining is carried out to evaluate the cell viability using fluorescent microscopy and, in order to prove the 3-Dimensions structure of in vitro alveolar barrier, Z-stack images are analyzed.

1 Introduction

1.1 The pulmonary respiratory system

The respiratory system is a collection of organs that function in unison to enable the intake of oxygen and expulsion of carbon dioxide from the body. It is classified into two major parts: the upper region, which encompasses the nostrils, mouth, pharynx, and larynx, and the lower region, which includes the trachea, bronchi, and lungs. The nostrils and mouth serve as the entry points for the respiratory system, facilitating the ingress of air into the body. The air then flows through the pharynx, which is a muscular tube that leads to the larynx. Upon entering the larynx, the air moves into the trachea, which is approximately 10-12 cm long and 2.5 cm wide. The trachea subsequently branches off into two primary bronchi, one for each lung. These bronchi further divide into smaller bronchioles, which, in turn, divide into alveoli. Alveoli are small air sacs located inside the lungs, where gas exchange between air and blood takes place thanks to the different pression between CO_2 and O_2. The lungs contain approximately 50 million alveoli at birth and about 480 million by adulthood and their region comprises about 90% of lung total volume [1].
Pulmonary circulation differs from systemic circulation, because it is characterized by thin-walled vessels and by less musculature. The pulmonary vascular tree begins as the main pulmonary artery and repeatedly bifurcates into arterioles and capillaries that cover 85–95% of the alveolar surface [2].

In this way pulmonary vessels can assist fast gas diffusion. There is an exceptionally thin membrane of only 1 μm between the alveolar gas and blood, allowing the rapid diffusion of the gases[3]. Indeed, the process of respiration serves the purpose of supplying cells with oxygen, needed for aerobic cellular respiration, thanks to inhalation, and removing the CO_2 produced by cells through exhalation [3].

This gas exchanger is characterized by a close relationship between the air spaces and the blood capillaries over a large surface area and across a minimal tissue barrier [4].

1.2 Physiological design principles of the pulmonary gas exchanger

The respiratory system can be categorized into two zones: the conducting zones and the respiratory zone. The conducting zones, which extend from the nose to the bronchioles, provide a pathway for the transportation of inhaled gases. On the other hand, the respiratory zone, which spans from the alveolar ducts to the alveoli, is where gas exchange occurs. [3].

The conducting airway of the lung is divided in 3 parts: the trachea, bronchi, and bronchioles. The tubes in this branched network get progressively smaller until they terminate with thin distal air sacs, called alveoli, which are closely associated with the capillary network to allow diffusion of oxygen into the bloodstream and removal of carbon dioxide [5]. In the walls of the alveoli (also called

alveolar-capillary barrier), a dense capillary network is connected to the terminal branches of pulmonary artery and pulmonary vein. The conducting airways and pulmonary arteries are designed to minimize both dead space and flow resistance; by contrast, in the gas exchanger part the air and blood volumes are maximized, thanks to the formation of alveoli that increase the surface-to-volume ratio, while the tissue barrier that separates air and blood is minimized [6]. The very thin alveolar tissue barrier that separates blood and air is comprised of two continuous cell layers, epithelium and capillary endothelium, and an interstitial space of variable composition and thickness between them [6]. The structure is shown in Figure 1.

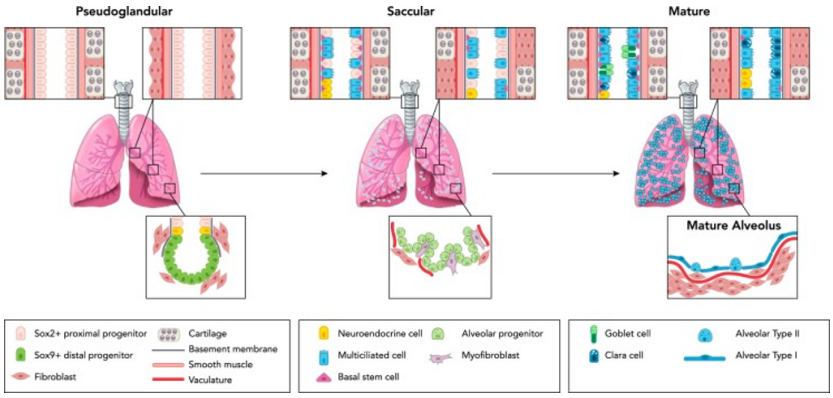

Figure 1: Development and anatomy of the human lung [5].

1.3 A single lung unit: The alveolar-capillary barrier

The gas exchange is due to the different pressure inside and outside the alveolus.The partial pressure of O_2 (PAO_2) in the alveolar gas (PAO_2) is much higher than in the capillary blood and O2 diffuses passively from the alveolar space into the blood during passage through the capillaries, until the pressure inside the alveolus equals that one outside in the capillary; meanwhile, the partial pressure of CO_2 (PCO_2) is greater in mixed venous blood ($\text{Pv}^{\bar{}}CO_2$) than in the alveolar gas (PCO_2) and diffusion over the alveolar–capillary membrane, therefore, results in a net flow in a direction opposite to that of O_2, from blood to alveolar gas [7], Figure 2.

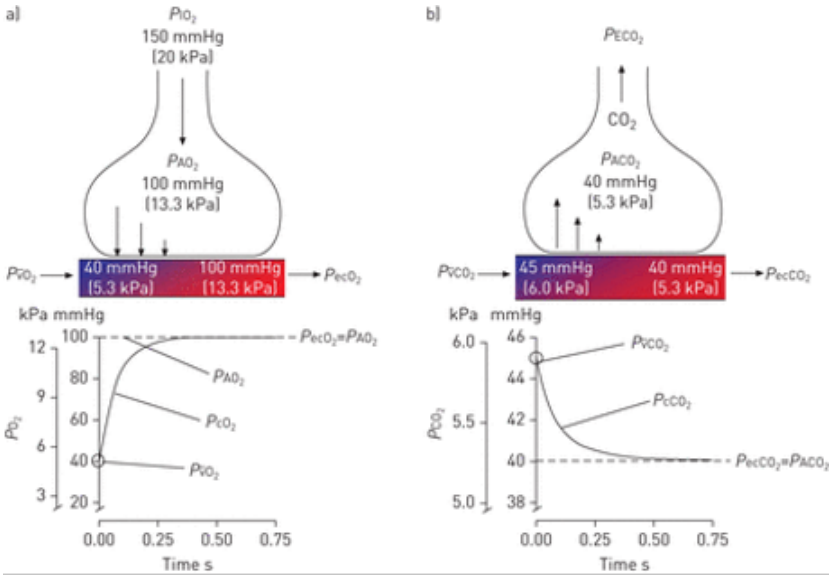

Figure 2: Gas exchange thanks to different pressure inside and outside of capillary [4].

1.4 The alveolar-capillary barrier: biological Membrane Conditions

The alveolar lung is characterized by a multitude of modulations and fine-tuning, such as varying the density of gas exchange surface or the thickness of diffusion barrier without compromising mechanical robustness of the microstructure or the overall organ. Instead, we can discern two different parts of the alveolar-capillary membrane: a thin interstitial space, where the two basement membranes are fused to facilitate the gas exchange, and a thick interstitial space, where the two basement membranes are separated to allow the formation of a slim interstitial space with the presence of fibroblasts and some connective

tissue fibers for mechanical support. The thin interstitial space is characterized by a basement membranes and some connective tissue fibers for the separation between the the endothelial cells (End) and the type-1 alveolar epithelial cells (EP1), Figure 3. In this part, there is also the presence of type-2 alveolar epithelial cells that secretes both the phospholipid and protein components of surfactant. But typer-1 cells (EP1) cover 95% of the alveolar surface [6].

The thick interstitial space assure the mechanical robustness of the microstructure thanks to an an interstitial space of variable composition and thickness between epithelium and capillary endothelium, this part is composed by a slim interstitial space rich in fibroblasts and some connective tissue fibers for mechanical support [6].

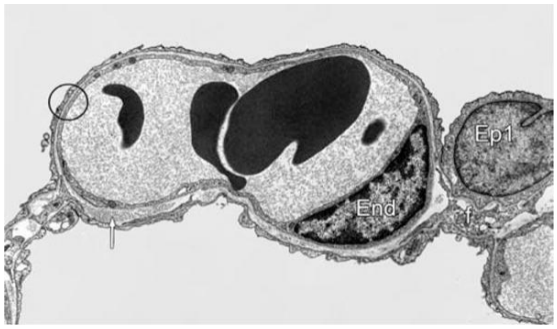

Figure 3: The alveoli are lined by epithelial cells, here a type-1 cell (Ep1), which are separated from the endothelial cells(End) by a single fused basement membrane in the upper part(circle) [6].

Despite its main function is to ensure the gas exchange, the alveolar epithelium is not directly exposed to air but covered by a surface film and an aqueous hypophase, where surfactant is present and constitutes the surface film at the air–liquid interface [1]. The mature alveolar epithelium consists of type I (AECI) and type II (AECII) alveolar epithelial cells, that occupy respectively about 95% and 5% of the surface. The AECIs provide the thin surface of the alveolus [8] and the AECIIs are large cuboidal cells that secrete active substances on their surface; AECIIs are widely referred to as 'alveolar stem cells' and contribute toward lung repair and regeneration [9].

The alveolar epithelium has different mains roles:

- to provide an extensive surface for gas exchange, this is supported by the alveolar epithelium that represents 99% of the surface area of the lung. During inspiration, this surface can reach 150 m^2 and this is made possible by the presence of almost 500 million small bubble-like alveolar components [8].
- to protect from environmental insults by secreting inhaled foreign agents and regulating water and ions transport that contribute to the maintenance of alveolar surface fluid balance [8].

- to regulate the production of the pulmonary surfactant that allows mechanical stability of the membrane during breathing and constitutes an important barrier that pathogens must cross to gain access to the rest of the organism via the respiratory [10].

- to permit a cross-talk between local cells and the lung immune and inflammatory response [8].

Underneath both the epithelial and endothelial cell layers, there is a basement membrane composed by a thickness of about 50 nm [11]. Those basement membranes are a permeable barrier with no general size of pores: the diameter is about 0.5-2.5 nm, with a small portion of larger pores characterized by a diameter of less than 400 nm [11].

In the thick portion of alveolar-capillary barrier, Figure 4, the two basements membranes, are divided by an alveolar interstitium composed by small fibrils of collagen, elastin and fibroblasts characterized by a stiffness of 1-2 kPa, measured as Young's elastic modulus, and with a total alveolar-capillary barrier thickness of 1.1 μm, instead the thickness of the air–blood barrier (alveolar-capillary barrier at the site of gas exchange) is smaller: thickness of 0.23 μm for the thick part and only 0.02 μm for the thin one [6],[11].

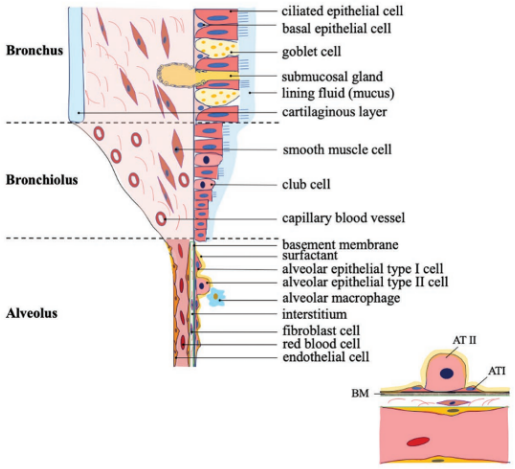

Figure 4: Schematic of cellular composition of the human airway tree from upper bronchus to alveolus [11].

1.5 Physiologic Stretch

A healthy lung normally inflates at a frequency of about 0.20 Hz, that is 12–15 inhalation-exhalation cycles per minute for rest conditions. This inflection causes the increasing of alveoli's size and surface area [6]. Under these respiratory conditions, the basement membrane, which represents the structural core of the air–blood barrier, is stretched to a linear strain of 4%, that can be reach 12% during deep inspiration and heavy exercise and 20% in pathological conditions [6]. This stretch with the mechanical stability is ensured by two components: a connective tissue fiber network and the surfactant system. The surfactant system is composed by about 90% of lipids and the last 10% of proteins. All of its components are synthesized, stored and secreted by type II alveolar epithelial cells. Its main role is to stabilize alveolar dimensions and to prevents alveolar collapse by a surface area-dependent reduction of alveolar surface tension [1].

1.6 The influence of mechanical stimuli on cells

Under physiological conditions, as breathing, the biological membrane with all the different cellular compartments in the lung face a continuous and dynamic cyclic mechanical stretch (21%, surface area), mainly a result from inspiratory inflation, expiatory deflation and pulsatile blood [6].

This mechanical stretch has an important role in the cell proliferation, cell differentiation, surfactant secretion. In addition, cyclic stretch can alter cell morphology of alveolar epithelial cells. For example, in this review [12], the gene transfer and expression of reporter plasmid DNA has been enhanced in human pulmonary A549 cells thanks to the application of a moderate equibiaxial cyclic stretch (10% change in basement membrane area, 0.5 Hz, 50% duty cycle) that made possible a cytoskeletal reorganization encouraging the gene therapy. There was a significant reorganization of the microtubule network after 24 hours of cyclic stretch: Figure 5 a) shows that tubulin in the TX-100 insoluble fraction (i.e. polymerized tubulin) decreased significantly over time with stretch, indicating a depolymerization of the microtubule network; this result was confirmed by immunofluorescence microscopy, Figure 5 b, where fewer microtubules were seen (right panel) compared to unstretched control (left panel).

Moreover, a high deformation can active intracellular signaling pathway that could disrupt the tight junctions affecting the way that micro-molecules have to across the alveolar epithelium [6]. For example, an excessive cyclic cell stretch (30%, surface area) for up to 48 h upregulated the production and release of cytokines, especially inflammatory mediators such as interleukin-8 (IL-8) [13]. Furthermore, mechanical stimuli also induce apoptosis, phosphatidylcholine secretion, necrosis in alveolar type II cells [14] and may therefore promote processes such as angiogenesis, proliferation, inflammation, apoptosis, vascular tone and cell survival [11].

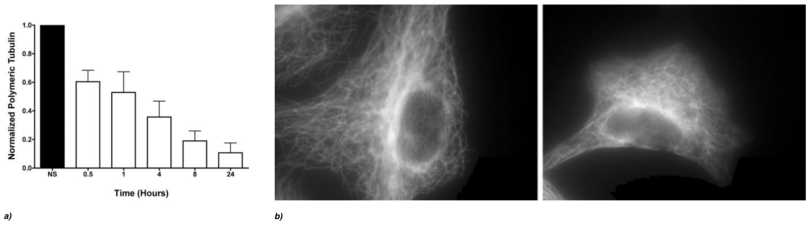

Figure 5: Cells were removed from the stretching environment at t = 0.5, 1, 4, 8 or 24 hours and allowed to grow under static conditions out to 24 hours, at which time the protein containing either total tubulin or polymerized tubulin was extracted. a) Densitometry measurements for polymeric tubulin relative to unstretched controls, b) after stretch for 24 hours (right panel) and compared to unstretched controls (left panel)[12].

1.7 Pathological conditions

Respiratory diseases are the leading causes of death worldwide [6]. The respiratory system is exposed to damaged substances during inhalation and exhalation, such as dust and soot, mould, fungi, bacteria and viruses. For this reason, one of the mains roles of the alveolar-capillary barrier is to defend itself from these harmful substances thought a complex mechanism of defense. The major role in the defense mechanism is made by alveolar macrophages, a type of white blood cell on the surface of alveoli, that seek out deposited particles, bind to them, ingest them, kill any that are living, and digest them. Together with alveolar epithelial cells, they provide the immediate response to toxic substances and pathogens that reach the lower respiratory tract [15].

Diseases associated with alveolar epithelium dysfunction include the idiopathic pulmonary fibrosis (IPF) that is a chronic disease characterized by alveolar epithelial cell dysfunction or a reprogramming, which leads to abnormal fibroproliferation in the lung, it is also a progressive disease because with the time the dense scar tissue takes the place of normal lung tissue [16].

Between airway and systemic inflammatory diseases there is the Chronic obstructive pulmonary disease (COPD) that is caused by a persistent obstruction of the airflow in the lungs and it is the third cause of mortality worldwide by 2030 [17]. It can be caused by emphysema, where the pulmonary air sacs are damaged, or by chronic bronchitis characterized with a continuous airway inflammation. [17]. Individuals who have high levels of exposure to tobacco or to other harmful chemicals as well as individuals with alpha-1-antitrypsin deficiency are more prone to developing COPD [17].

Inside the diseases associated to an excessive alveolo-capillary permeability, it can be classified the Acute respiratory distress syndrome (ARDS) that is defined by the acute onset of noncardiogenic pulmonary oedema, hypoxaemia and the need for mechanical ventilation [18]. It occurs when fluid builds up in the tiny elastic air sacs (alveoli) in the lungs; this fluid takes the place of the

air that means less oxygen. Normally, a protective membrane keeps this fluid in the vessels.

Generally, an excessive alveolar-capillary permeability is one of the major pathological characteristics of acute lung injury [15].

Coronavirus disease is a systemic disease associated with vascular inflammation and endothelial injury. For the infection of the endothelial cells (ECs), once it reaches the alveoli of the lung, the virus uses the receptor the angiotensin converting enzyme 2 (ACE2) that bonds with the protein Spike of the virus. This link allows the release of RNA viral genome inside the ECs. After the infection, ECs are characterized by significant cytoplasmic disruption, dissolution of gap junctions and separation from the basement membrane [19].

1.8 Lung models

The following sections will be dedicated to a comparison between the main types of models used in biomedical research, with a focus on lung and alveolar-capillary barrier models.

1.8.1 Animal models and limitations

Animal models are enormously used in biomedical research thanks to their capacity to mimic human condition and its complexity in terms of circulatory factors, hormones, cellular structures, and tissue systems. Generally, animal models are very useful for understanding and predicting physiological and therapeutic outcomes that are used in various fields of regenerative and tissues engineering. The most important criteria are the proper selection of models in terms of resemblance between animal species and humans in terms of physiological and/or pathophysiological aspects [20], but also choosing the appropriate animal model associated with economic costs that can be afforded [21]. In vivo models are mostly conducted in mice, rats, and rabbits for its lowest possible position in the evolutionary scale while still being compatible with a good degree of similarity with the human species. For example, transgenic minces are used to study the Gram-negative bacteria genus Neisseria that colonize mucosal surfaces and the oral cavity of humans and many animals [22]. Transgenic minces are also used to study Alzheimer's Disease [23].

Despite the similarities between the animal and the human organism, there are obvious differences between the two organisms. For example, in human organisms the cell turnover is very low and the airway progenitor cells are quiescent, while inside the mice the proliferation and phenotype of cells can change in response to certain injury: an example is Alveolar epithelial type 1 cells (AEC1), this cell type normally has a limited proliferative capacity in vivo, but in specific injury mice models they have shown the ability to proliferate and give rise to Alveolar epithelial type 2 cells (AEC2) cells [24], [25].

1.8.2 The 3R principles

According to the Directive 2010/63/EU, the Europe wants to follow a guiding principle for animal experimentation called "the 3R principles": Replacement, Reduction, Refinement.

- Replacement: Directive 2010/63/EU contains the following major clause "An experiment shall not be performed if another scientifically satisfactory method of obtaining the result sought, not entailing the use of an animal, is reasonably and practicably available", in other words there is a wide range of well-established and emerging methodologies as alternatives for the absolute replacement of animals.

- Reduction: when the replacement of animals is not possible, Directive 2010/63/EU suggests to reduce the number of animals involving in experiments.

- Refinement: when every effort has been made to reduce the number of animals for experimentation and replacement is not an alternative, it the moment to pass into refinement that refers to the decrease in the incidence and/or severity of inhumane procedures applied to animals while participating in experimental protocols to minimize the pain and distress and to enhance welfare.

Historically, the 3R have been advocated for social and ethical reasons, with less focus on how they can contribute to advances in research itself. For this reason, in the last years there have been an expansion of the 3R to the 5R, to include "Rigour" and "Reproducibility". This addition may provide a higher reduction in the use of animal: Rigour in adding more detailed descriptions of experimental procedures, animal welfare measures, housing conditions and this transparency in reporting methods, experimental desing and their results could help to improve refinement and the welfare of animals and enhance Reproducibility [26].

1.8.3 In silico models

Understanding how developmental systems evolve over time is a key question in biomedical and medical research, in recent years, we have been constructing in-silico models that synthesize experimental knowledge using software engineering tools. Otherwise, in silico medicine is the use of computational modeling simulation in medicine to make easier the prevention, diagnosis, prognosis and treatment planning of diseases. Computational methods can quantify physical quantities that are difficult or impossible to measure directly. The critical point of in silico medicine is that this model should be robust enough to provide a trust description of what happens in reality. For example, in silico models have been used to study cancer, in this case in silico medicine is very useful because it can be involved biological interactions across diverse physical, temporal, and biological scales [27]. These in silico approaches are also used to improve the

drug design and to optimize the delivery of drugs to target sites in the host tissue [28].

The in silico models are also useful to estimate human parameters inside the organ. For example, it can be used to map the pressure of conductive branches during inspiration and expiration, Figure 6 [29].

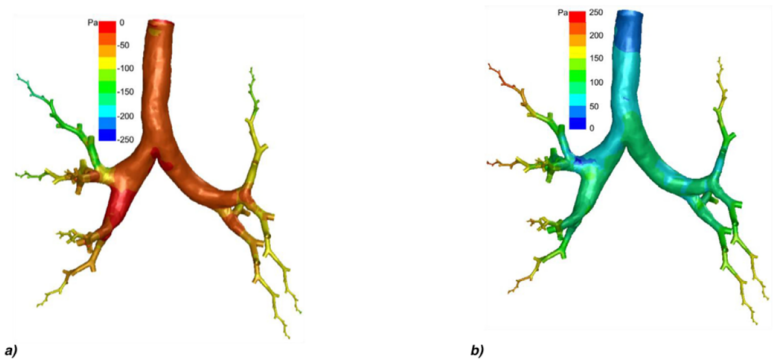

Figure 6: a)Pressure contours for a flow rate of 65 L/min in inspiration and b) in expiration [29].

Moreover, computational simulations of lung airflow may contribute to cost reduction and improved outcomes [29].

1.8.4 In vitro models

In vitro models include 2D cell cultures that can be cell monolayers or co-cultures, 3D cultures like spheroids, organoids or assembloids; microfludic devices like organ-on-a-chip. The use of these models allows to overcome ethical problems connected with animals used inside experiments, as well as they can be reduced the cost inside the research. Moreover, in vitro systems offer tightly controlled cellular environments that can be evaluated in real time.

1.8.5 Two-Dimensional (2D) cell culture models

The first basic in vitro models are based on a culture of cell in a 2D condition. 2D monolayer cell culture has been used for decades because it is easy to maintain and can expand with little cost. However, 2D models do not mimic in vivo conditions due to the missing of the tridimensionality. For this reason, preclinical testing with 2D cultures are not predictive for different reasons: cells in 2D are constantly exposed to high levels of nutrients and oxygen, parameters that, in vivo, are subject to variability imposed by the environment. More in general, cell lines do not recapitulate certain in vivo conditions such as peculiar cell–cell and cell–matrix interactions. For example, in this review [30], it has

been analyzed how using two-dimensionally (2D)-cultured cell lines is unable to precisely select clinically active oncology drugs because, once cell lines were seeded, there wasn't the developing of dense multicellular spheroids (MCSs), so there was a smaller resistance to paclitaxel and doxorubicin compared to the three-dimensionally (3D)-cultured cell lines. In this scenario many drugs could work in a culture dish but ultimately fail in the clinic.

1.8.6 Air-Liquid Interface

The alveolar epithelium of the lung constitutes a unique interface with the outside environment. For this reason, submerged in vitro models are not predictive. Submerged in vitro models lack the physiological features of alveolar-epithelial barrier that includes both endothelial and epithelial cells with the requirement of the epithelial barrier exposed to the air. This is fundamental to mimic the inside of alveolus. To overcome the drawback related to physiological relevance of human alveolar-epithelial barrier, more complex models have been created with cells kept in Air-Liquid Interface (ALI) condition. ALI allows to generate biomimetic airway epithelial cell culture and it takes the main role in the study of several pathogens connected to the gas exchange, like SARS-coV-2 [31]. To create the Air-Liquid Interface, Human airway epithelial cell (hAEC) are expanded on a porous membrane insert (transwell). After 2-4 days, once cells have reached confluency, is the moment of differentiation induced by removing the liquid medium. After complete differentiation, it appears a pseudostratified, polarized epithelial layer including ciliated cells, club cells, goblet cells and basal cells, Figure 7 [31].

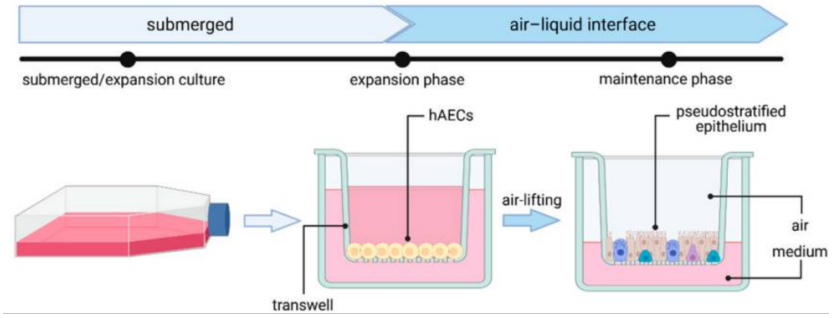

Figure 7: Generation of human airway epithelial cell culture in air-liquid interface (ALI) from human airway epithelial cells (hAECs) [31].

ALI is also used to study inflammatory and oxidative stress responses of Alveolar Epithelial Cells after airborne nanoparticles of Zinc Oxide inhalation. This review [32] compares the ALI model with the submerged model (where the toxin/stressor is dissolved or suspended) directly in the cell culture medium covering the cells. The last model has 2 mains problems: first of all, it is unrealistic and artificial environment for alveolar epithelial cells in the lungs, secondly

it is more difficult the quantification of NPs that reach the cells, this problem is higher when there are small particles and the diffusion along the membrane becomes the dominant transport mechanism, Figure 8 [32]. Furthermore, the ALI condition gives more biomimetic particle deposition rate: under ALI conditions, the rate of particle deposition onto the cells remained constant (within 20%) throughout the 3-hour exposure time by maintaining the sample flow and ZnO aerosol concentration. While, under submerged conditions, the size of ZnO particles increased from a mass median diameter of around 350 nm to approximately 900 nm within 30 minutes due to agglomeration, resulting in a threefold increase in deposition rate. This means that the entire ZnO dosage is delivered to the cells within approximately an hour [32].

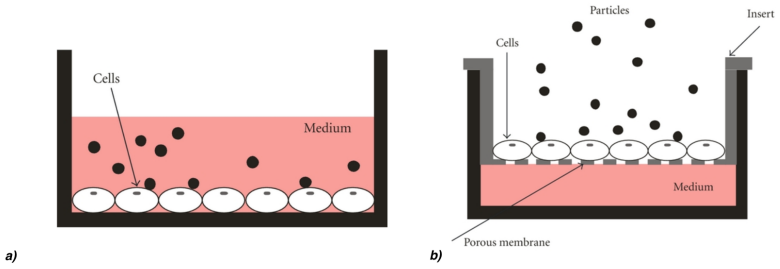

Figure 8: Schematic of the two cell exposure models used for studying particle-cell interaction. (a) Exposure at the air-liquid interface (ALI): airborne particles are directly deposited on cells grown at the air-liquid interface. (b) Exposure under submerged conditions: particles were suspended directly in the cell culture medium covering the cells [32].

Then, the ALI conditions are more physiologic than the submerged ones because they allow to polarize the epithelial cells, mimicking the epithelial barrier's function. To reproduce this condition, epithelial cells are typically cultivated on a porous membrane (usually polyethylene terephthalate, PET) with cells exposed to the air on the apical side and to the medium on the basal surface, Figure 9 [11].

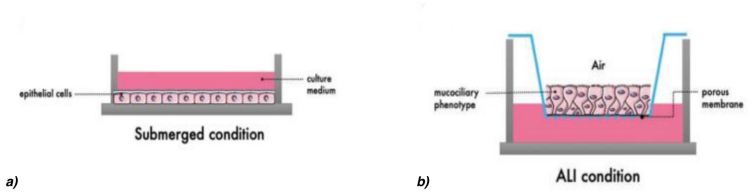

Figure 9: a) *In vitro* cell culture model under submerged condition; b) *In vitro* static cell culture model under ALI condition using Transwell inserts [11].

1.8.7 Co-Cultures

Monocultured cells are not representative of the alveolar-epithelial barrier architecture and complexity whose functionality depends mostly on the co-presence of endothelial and epithelial cells.

In this review [33], they have analyzed how the crosstalk between co-cultures of A549 cells and THP-1 cells can reduce the oxidative stress due to cigarette smoke (CS). Indeed, the monoculture of A549 cells showed that, after 24h, the cytotoxicity was about 48%, while if A549 cells were kept together with THP-1 cells, the cytotoxicity decreased to 24%. So THP1 had the role to protect A549 cells from the cytotoxicity of CS and the co-culture shows a better simulation of what in vivo happens.

First of all, the permeability of the barrier changes in case of monocultures or co-cultures, as demostrated by Pasman et al. [34] that compares the electrical resistance and the permeability in case of only human lung microvascular endothelial cells (LMVECs), only Calu-3 cells (derived from human bronchial adenocarcinoma) or co-cultures of both cells types, Figure 10 shows the higher electrical resistance and lower permeability when both cells are cultured on Porous Poly(Trimethylene Carbonate) Membrane.

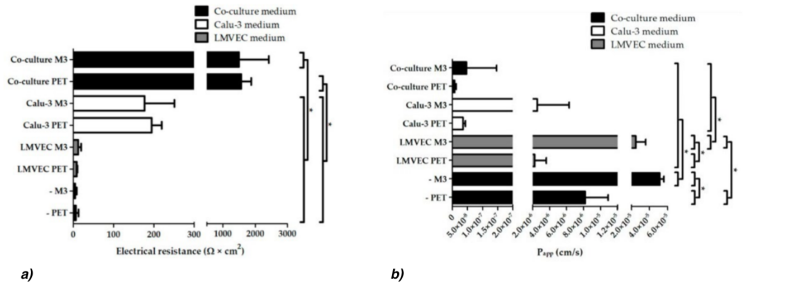

Figure 10: (a) Electrical resistance and (b) FITC-dextran permeability assays were performed on inserts with M3 or PET membranes containing either no cells, Calu-3 cells, LMVECs, or co-cultures [35].

1.8.8 Tri-Cultures

In human airway barrier, there is an interstitium rich of fibroblasts, for this reason it becomes interested studying how these three cells types work together. In this review [35], the behavior of epithelial, endothelial cells with fibroblasts has been analyzed on a native collagen membrane to reproduce the buccal mucosa. Co-cultures and tri-cultures were generated by placing the collagen membrane (6 mm diameter) in cell culture inserts for 24 well plates. This the collagen membrane has been used as a scaffold with a porous side where endothelial cells and one day later fibroblasts were seeded on the porous side; after cultivation

with endothelial cells and fibroblasts for three days the collagen membrane was carefully turned upside-down and seeded with epithelial cells.

The results, Figure 11, show an epithelial layer on the upper side of the collagen membrane, a deep infiltration of fibroblasts from the bottom side, and superficially-formed capillary structures by microvascular endothelial cells exhibiting a lumen size between 10 and 30 μm [35]. The co-presence of epithelial, endothelial cells and fibroblasts is essential to analyze how the alveolar-capillary barrier works.

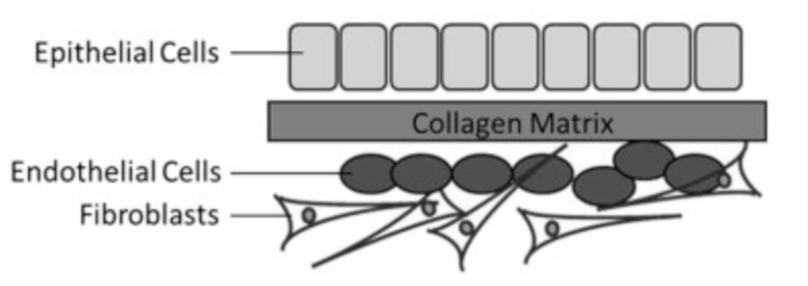

Figure 11: Scheme of pre-vascular buccal mucosa: epithelial cells, fibroblasts, endothelial cells besed on a natine collagen membrane [35].

1.8.9 Bioreactors in tissue engineering

Several existing systems allow the examination of large sections of lung tissue ex vivo, but only for a limited period of a few hours within the laboratory setting. To overcome this problem, bioreactors are used to provide a tissue-specific physiological in vitro environment during tissue maturation over long durations (several days), [36]. Moreover, they are used to mimic in vivo condition and to control cell culture parameters (e.g. temperature, cell density, media renewal rate). In this paper [37], the final bioreactor design is capable of supporting the culture of whole native lung tissue for up to 1 week in the laboratory. The tissue was a lung harvested from young adult (3 month-old) male rat. The bioreactor is composed by a central chambre to contain the lung, this main chambre is connected with a second chambre, " tracheal reservoir", that can be filled with culture medium to allow ventilation with medium, or can be empty to enable ventilation with air, Figure 12.

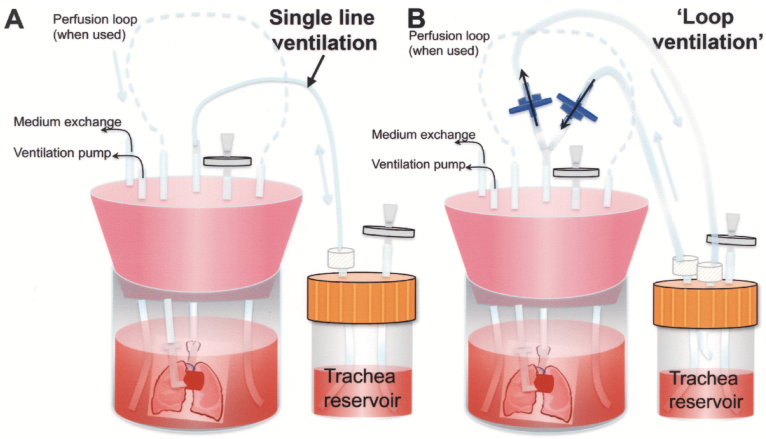

Figure 12: Bioreactor schematic diagrams: A)schematic showing single ventilation; B)schematic showing a "loop" ventilation [37].

In this paper [38], they developed a decellularized murine lung matrix bioreactor system that could be used to evaluate the potential of stem cells to regenerate lung tissue. Following the process of decellularization, a small tube was introduced into the trachea of the matrix and sutured in position with silk thread. The cannula was attached to a ventilator to simulate normal, murine breathing-induced stretch ventilation (180 breaths/minute; 300 μL volume) and placed in a 37°C, 5% CO2 incubator, Figure 13.

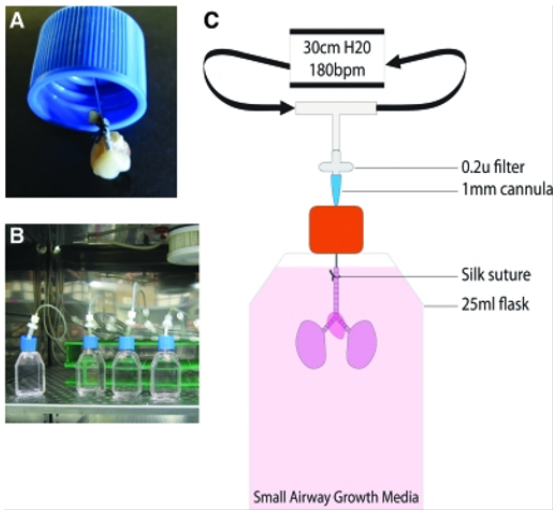

Figure 13: Setup of decellularized lung matrix bioreactor system: Depiction of how the cannula is inserted through the filter cap into the trachea of the decellularized lung and tied in place with silk suture; (B) The matrix is suspended in a flask filled with the small airway growth medium, and the cannula is attached to a ventilator (room air) to simulate normal, murine breathing-induced stretch and placed in a 37°C, 5% CO2 incubator. (C) Schematic of bioreactor setup [38].

Moreover, tissues in the body do not exist in isolation, but reside in a highly integrated and dynamically interactive environment. For this reason, several systems can be connected each other to recreate a body-on-chip to study multi-organ physiology and, for example, to correctly reproduce the response of the chip to drugs. In this review [39], they analyzed three-tissue organ-on-a-chip system, comprised of liver, heart, and lung (figure) to observe drug responses that, as already mentioned, depend on inter-tissue interaction. Each tissue model was created with the cell types present in the native human tissue: while the heart and liver organoids were obtained by bioprinting spheroids and culturing them in suspension conditions, the lung model consists of a co-culture of pulmonary epithelial cells and pulmonary fibroblast layered on a side, and endothelial cell on the other side of a porous membrane. Once all the constructs were mature, they were connected into the same circulatory flow to be subjected to perfusion, Figure 14.

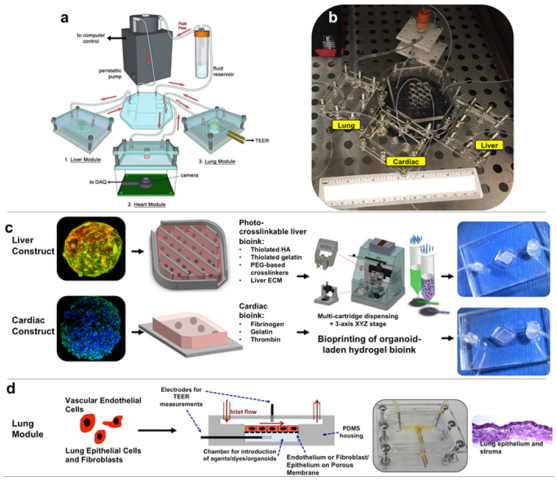

Figure 14: Overall design and implementation strategy for the 3-tissue-representative organ-on-a-chip system using a variety of biofabrication approaches: a,b)Illustration and photograph of the modular multi-tissue organ-on-a-chip hardware system set up for maintenance of 3 tissue model: liver, heart and lung; c,d) General overview of how each tissue type is prepared for the system [39].

1.8.10 Microfluidic approaches

Microfluidic devices can be separated into active and passive devices: passive microfluidic devices are geometry-dependent, while active microfluidic devices include sensors or detectors that transduce chemical, biological, and physical changes into electrical or optical signals, [40]. Microfluidic devices have many advantages, as it can be seen in the Figure 15. First of all, the cost for the production is minimal due to the small dimension, for the same reason the use of reagents is low. Furthermore, the microchannels' size (in the order of a few micrometers with a volume of $10^{-9}L$ to $10^{-13}L$), that enables a low Reynold number, allows to have a laminar fluid, resulting in more precise and accurate results, offers a faster reaction time due to the lower diffusion inside the microchannels, increases the velocity of the response, allows to put on the single chip more than one assay making possible an high throughput, [41]. Moreover, the devise's size (in the order of a few centimeters) makes it easy to portable.

Microfluidic device support dynamic culture condition that is essentially also for angiogenesis and cell migration and make the fluidic conditions similar to those found in vivo. So, it is a better biomimetic device than the models previously discussed. Various materials can be used in the fabrication of a microfluidic device such as inorganic materials (like silicon or glass), organic materials (like paper) and polymers that are most extensively used due to their ease of access, low cost, flexibility and superior biochemical performance [41].

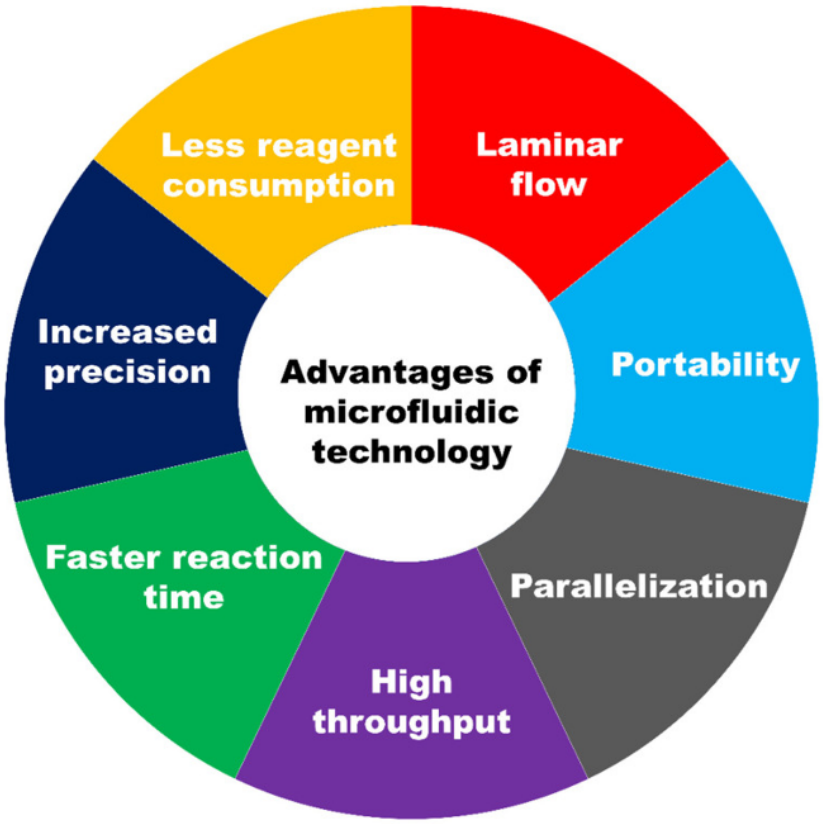

Figure 15: Schematic showing various advantages of microfluidic technology [40].

1.8.11 Fabrication of organ-on-chip

One of the commonly used material for the manufacture of microfluidic devise is the Polydimethylsiloxane (PDMS), consisting of a polymeric chain with repeating Si-O groups and CH3 groups on the side. It has many advantages for the biomedical field, Figure 16, such as its transparency, flexibility, biocompatibility and gas permeability. It is also optically transparent and non-fluorescent, that make it compatible with monitoring techniques. Futhermore, it has a simple fabrication by replica moulding, chemical stability and it is simple to handle and its production is easier and less expensive than other materials [42], [43].

The most famous techniques to obtain the molds are:

- Soft lithography is a technique for fabrication using elastomeric master. It is called soft because it uses elastomeric materials like PDMS for the master. This one is obtained through traditional lithography: transfer a precise design from a mask on a polymer layer (resist) coated on the

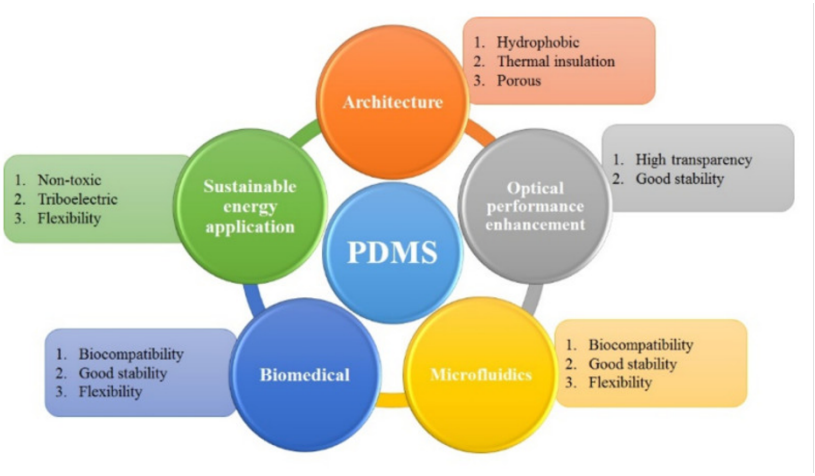

Figure 16: The PDMS applications corresponding to its properties [42].

substrate you want to change. There is a mask that allows or not the passage of UV rays or X rays. The mask that could be positive or negative: positive if solubility in areas exposed to radiation increases after the rays' exposition and those parts will then be removed; negative if the part of the resist not impressed by rays are removed after the exposition. After the development, where the excess of resist is removed, the result is a wafer with a tri-dimensional pattern. Then this 3D pattern will be used to obtain an elastomeric master, most notably a PDMS master. Soft lithography is the most common approach for rapid and low-cost fabrication of microfluidic devices for medicine, biology, and chemistry.

- Laser micromachining or ablation technique is a thermal technique where the large temperature gradient easily leads to the distortion of PMMA material during laser ablation through the melting, decomposing, and then vaporizing from the molten material. In this way it can be obtained the geometry wanted [43].
- Additive manufacturing techniques, like fused deposition modelling, stereolithography, PolyJet and 3D printing, are techniques that allow to obtain molds layers-by-layers using computer-aided design [44].

Once the molds are obtained, the elastomeric solution is casting inside the mold and cured in the oven. After the curing process, the piece is taken out of the mold. This technique is called "Cast-molding" and the main advantage is that the mold could be used repeatedly to prepare the PDMS structures without compromising their quality [45].

1.8.12 Organs-on-Chip

The inadequate comprehension of the fundamental pathophysiology and underlying mechanisms of human diseases is a primary cause for the high rate of new drug failures during clinical trials. Organ-on-a-Chip has the potential to be used as a substitute or alternative modeling system for animal models, as it can aid in the discovery of crucial pathological mechanisms and the identification of therapeutic targets and biomarkers for enhancing disease outcomes [46].

The Figure 17 shows microfluidic form of microphysiological system in various sizes and shapes.

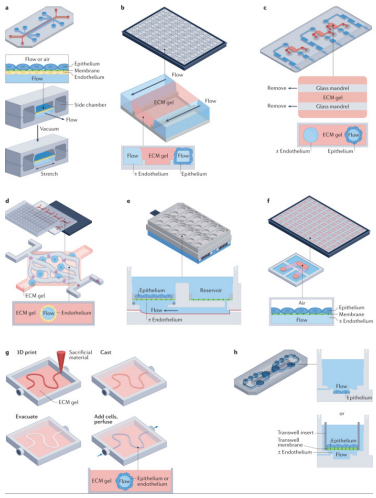

Figure 17: Microfluidic devices [46].

In our case, alveolus- on-chip would face the challenge of developing a device able to support both the presence of an air-liquid interface (ALI) in the apical compartment of the device and the presence of a tri-culture cells to mimic the natural environmental of alveolar-capillary barrier. Moreover, the implementation of a mechanical stimulation of the barrier model would recapitulate the effects of the breathing motion on the physiological tissue.

Lung-on-chip could be used in submerged or ALI conditions: device containing a submerged condition are less representative on the in vivo setting. For implementing ALI condition, there are different ways, Figure 18: in standard 2D-colture cells where media is simply removed from the top compartment after a period of cells adhesion and the lung-on-chip device where ALI can be operated in dynamic or semi-dynamic more where there is a porous membrane, that mimics the submucosal layer, placed between two different canals, the upper channel to create the air condition and the lower channel to mimic the blood flow [47].

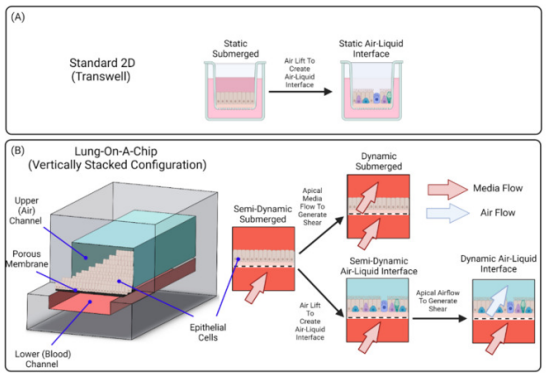

Figure 18: Air–Liquid Interface Configurations: (A) Standard 2D ALIs require simply removing media from the top compartment while; (B) ALI in lung-on-a-chip devices can be operated in semi-dynamic or dynamic mode [47].

Since lung-on-chip models can mimic many aspects of the human environmental, they also can be used to study respiratory diseases. In this review [48], with the use of a gut-on-chip, it has been analyzed the intestinal responses after SARS-CoV-2 infection. The human intestinal model presents two different channels that are separated by a thin (25 μm) PDMS membrane with through holes to build tissue-tissue interfaces, Figura 19.

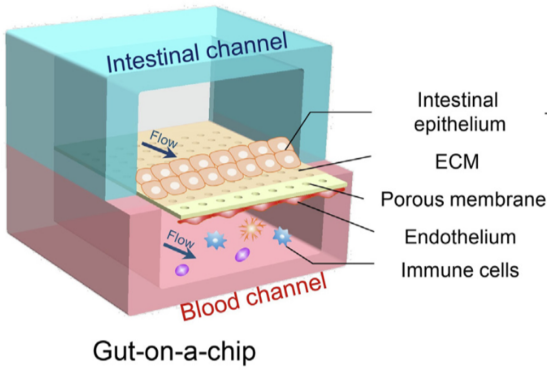

Figure 19: The configuration of the multilayered intestine on the chip device infected with SARS-CoV-2 [48].

Before cell seeding, both sides of the porous membrane were coated with type I rat tail collagen. In the upper channel, the intestinal epithelial Caco-2 cells and HT-29 cells secreting intestinal mucin were seeded under static culture for 2 hours, while in the lower channel human umbilical vein endothelial cells (HUVECs) and immune cells were seeded to create the vascular endothelium.

Once the attachment has been ensured, the culture become dynamic for 5 days and, for the infection with SARS-cov-2 the human intestine model, the upper intestinal canal of the chip device was infused with 30 μl of DMEM containing high glucose virus at a MOI of 1, [48]. As confocal micrographs shown, after 5 days of co-culture, intestinal epithelial and endothelial cells formed confluent monolayers under fluid flow, thus forming an epithelium-endothelial intestinal tissue barrier demonstrated by ZO-1 and VE-cadherin formation, Figure 20 a,b. In particular, the epithelial cells formed structures similar to villi, Figure 20 c) and the Figure 20 d shows as MUC2 had an ability to secrete mucus under fluidic flow.

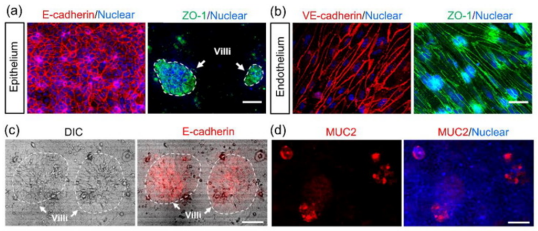

Figure 20: Characterization of the intestinal epithelium and endothelium in the human gut-on-chip:a) Confocal micrographs of the intestinal epithelial barrier on the chip visualized by the expression of an adhesion junction (E-cadherin) and tight junction markers (ZO-1). The intestinal villus-like structures with high levels of ZO-1 expression are indicated by white dashed lines; b) Confocal micrographs of the vascular endothelium identified by the expression of an adhesion junction protein (VE-cadherin) and ZO-1; c) DIC image of an intestinal villus-like structure with clumps of cells (indicated by white dashed lines); d) Immunostaining of a mucin marker (MUC2) in intestinal epithelial cells [48].

About the virus, the SARS-cov-2 infection on this gut-on-chip system caused the interruption of the villi (Figure 21 a), the distruption of the integrity of the intestinal barrier (Figure 21 d), the alteration in the secretion of mucus (Figure 22 a), the reduction of cell density and size (Figure 22 c and d).

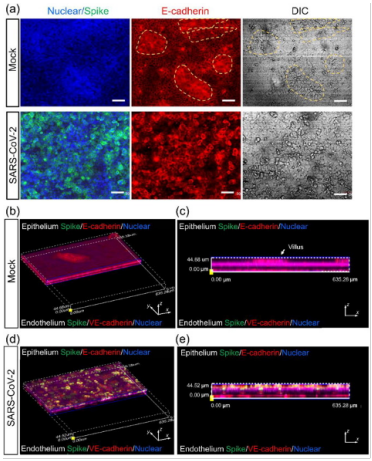

Figure 21: Examination of SARS-CoV-2 infection in the human gut-on-chip system: (a) Confocal micrographs of SARS-CoV-2 infection (Spike protein) on the intestinal epithelium (E-cadherin) and intestinal villus-like structures (indicated by yellow dashed lines) at day 3 post-infection; b, c) The 3D reconstructed confocal image and side view of a mock-infected gut-on-chip; d, e) The 3D reconstructed confocal image and side view of the virus-infected intestinal model [48].

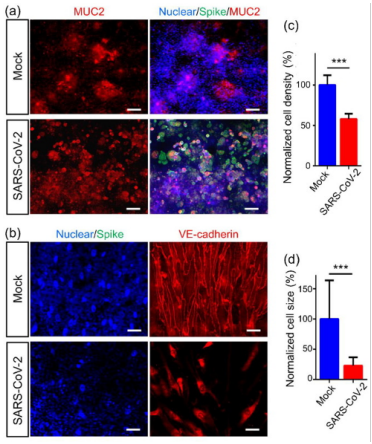

Figure 22: Morphological changes in the intestinal barrier on the chip after viral infection: (a) Confocal micrographs of SARS-CoV-2 infection and MUC2 expression in the intestinal epithelium at day 3 post-infection; b) Confocal micrographs of viral infection (Spike protein) in the vascular endothelium (VE-cadherin);c, d) Quantification of endothelial cell density and size for mock- and SARS-CoV-2-infected chips [48].

Another example of lung-on-chip has been analyzed in this article [49] Zhang et al. investigated the immune response to SARS-CoV-2 infection.

The system described in Figure 23 consisted of a porous membrane coated with extracellular matrix (ECM), allowing for the co-culture of human alveolar epithelial cells, pulmonary microvascular endothelial cells, and immune cells between two perfused channels - the alveolar lumen and vascular channels. The top channel was utilized to infect the barrier model, while immune cells were introduced into the vascular channel to investigate the pathological changes of the epithelium-endothelium interface and inflammatory responses following virus infection. In this study, the team treated the virus-infected human alveolus chip with Remdesivir, which was found to effectively suppress virus replication and reduce virus-induced damage to the alveolar-capillary barrier.

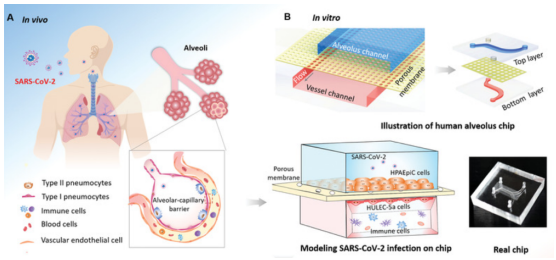

Figure 23: Schematic diagram of microengineered human alveolus chip infected by SARS-CoV-2: A) Illustration of 3D human alveolar-capillary barrier in vivo; B) The configuration of biomimetic human alveolus chip infected by SARS-CoV-2 [49].

1.8.13 Mechanical stimulation of the barrier model

Mechanical stretch has been shown to modify cell regulation, proliferation and differentiation. For this reason, the presence of mechanical stimulus is mandatory when physiological response must be studied. The microfluidic device employed in this study [50], referred to as the "human alveolus chip," comprises of two parallel channels. These channels are divided by a porous membrane coated with an extracellular matrix (ECM) and are lined with primary human lung alveolar epithelium cells. These cells are cultured under an air-liquid interface (ALI) on the upper surface of the membrane, while primary human pulmonary microvascular endothelial cells are present on the lower surface. The lower channel is continuously supplied with culture medium to provide nourishment to the endothelial cells, Figure 24.

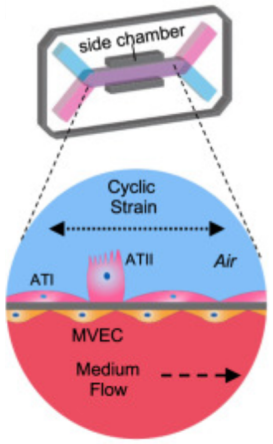

Figure 24: Schematic of human alveolus chip with primary alveolar epithelial type I (ATI) and type II (ATII) cells lining the upper surface of the porous ECM-coated membrane in the air channel with and pulmonary microvascular endothelial cells (MVEC) on the lower surface of the same membrane in the basal vascular channel that is continuously perfused with medium [50].

In order to replicate the natural breathing patterns, the artificial connection between the alveoli and capillaries is subjected to periodic mechanical movements. This is achieved by applying cyclic suction to the hollow side chambers present within the flexible polydimethylsiloxane (PDMS) device, resulting in a 5% cyclic strain at 0.25 Hz [50].

One of the most known approach to stretc the membrane consists in the application of positive pressure to obtain the deformation on the air-liquid interface, as Radiom et al. [51] did in this paper where the models is an array of hexagonal monolayers of electrospun gelatin nanofibers suspended microframes and integrated in a microfluidic device, Figure 25. The suspended monolayers had a diameter of 500 μm a thickness less than 1 μm and were covered by a culture of A549 cells that have been subjected to a periodic strain of 5% due to air pressure of 200-1000 Pa with a frequency of 0,2 Hz for 1 hour to obtain a central displacement of 40–80 μm at the air–liquid interface. The added cell layer did not significantly alter the elasticity of the monolayer because the stiffness of the cell monolayer was much smaller than the stiffness of the gelatin monolayer, for this reason the combination of the two layers had an elastic modulus that was similar to the elastic modulus of gelatin monolayer (4 MPa), [51]. This strain reduced the coupling between cells and the nanofibers and induced remodeling of the actin cytoskeletron: the cells appeared to be less rounded, and their distribution on the gelatin monolayer appeared more homogenous in the samples subjected to the mechanical stimuli compared to the control, this means that the periodic strain may encourage cell migration towards less covered regions of the substrate, resulting in the formation of a tighter cell layer.

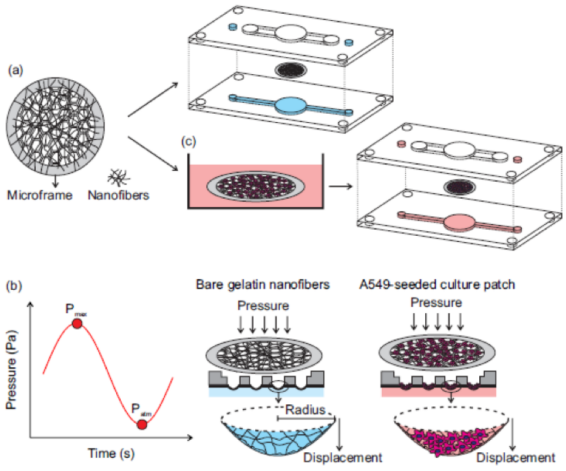

Figure 25: Displacement-pressure response of gelatin nanofiber monolayer together with fit to plate theory equation [51].

1.8.14 Alveolus-on-chip: background works

In vivo, as the Figure 26 shows, the alveolus air-blood interface is made by three lays across which gas occurs: there is a squamous epithelium in the air part, an endothelium in contact with the blood and these two cells type share a fused basement membrane, which allows for the minimization of the barrier across which exchange must occur.

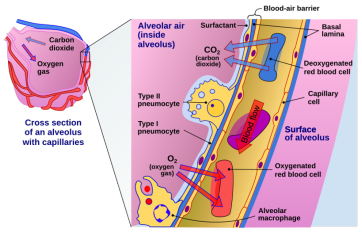

Figure 26: Structur of the alveolar-capillary interface [2].

An alveolar-capillary barrier in vitro model should include: cell types involved in the barrier, a stretchable substitute of the basal membrane, the air-liquid interface, perfusion and the shear stress for the endothelium and the cyclic mechanical stimulation that causes an average of 20% deformation with a frequency of 0,2 HZ [11]. In this work [52], the device contains two PDMS compartments separated by a thin porous membrane that reproduces the microarchitecture of the alveolar-capillary interface, as the Figure 27 d,e show with the formation of junctions lined by ZO-1 in the epithelium (Figure 27 d) and VE-cadherin in the endothelium (Figure 27 e).

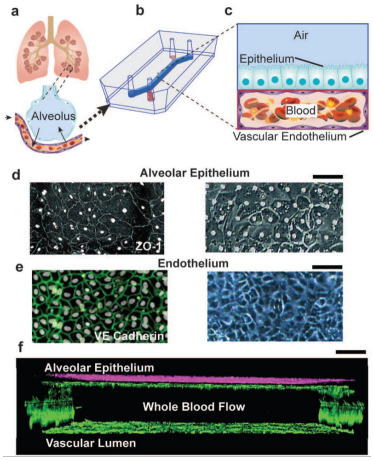

Figure 27: Engineering of an endothelium-lined tube within the alveolus chip [52].

A similar device has been used to study the SARS-CoV-2 infection that is firstly a pulmonary disease. [53] is a review in which a microfluidic alveolus chip is analyzed to study how the infection can attack the airways. The device contains an epithelial cell (ihAEpiC) culture channel where cyclic air mechanical strain can be induced to better mimic in vivo condition, endothelial cell (HUVEC) culture channel where continuous medium flow can be induced to mimic the blood flow, and central collagen I gel channel to mimic the stretchable substitute of the basal membrane, Figure 28.

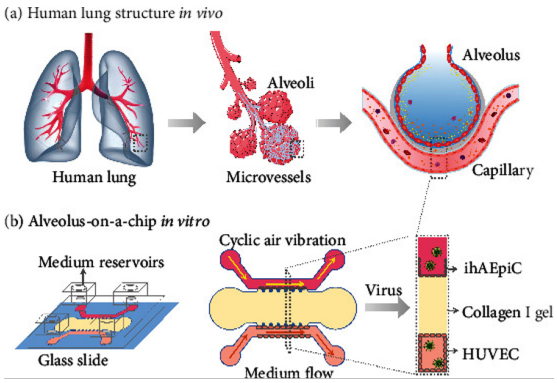

Figure 28: The 3D alveolus-on-a-chip platform: a) Schematics of the alveolus and alveolar-capillary barrier in vivo; b) Design and structure of the microfluidic chip [53].

The gold standard of the alveolar-capillary barrier is represented by the device by Huh et al. [54]. It is one of the first biomimetic microsystem that included the critical function of the alveolar-capillary human lung, especially for the presence of mechanical strain. The device is composed by three chambers and the central one is itself split into the upper chamber dedicated to the air and the low chamber to the medium flow, Figure 29. The PDMS porous membrane used to divide the central chamber is covered by alveolar epithelial cells and human pulmonary microvascular endothelial cells on the opposite side [54]. To recreates physiological breathing movements, in the two lateral chambers are connected by silicon tubes to a vacuum pump controlled by a software that allows to strain the PDMS membrane with a mechanical stretching of ranged from 5% to 15% to match normal levels of strain. Once the confluence was reached (¿ 2 weeks), the air was introduced into the epithelial microchannel and the alveolar cells were maintained at an air-liquid interface. Living Escherichia coli bacteria expressing green fluorescent protein was introduced in the medium flow, while neutrophils flowing in the vascular microchannel. The presence of these pathogens for only 5 hours was sufficient for the endothelium activation as indicated by neutrophils transmigration into the alveolar microchannel.

To test the inflammatory response of the lung-on-chip, its alveolar epithelial microchannel was exposed to silica nanoparticles for 5 hours, this type on

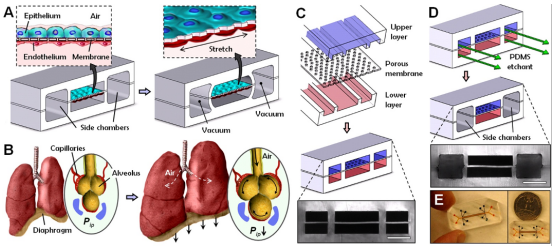

Figure 29: Biologically inspired design of a human breathing lung-on-a-chip microdevice [54].

nanoparticles are perfect to mimic the airbone particles. The result was that inflammatory cytokines was produced by the epithelial tissue and endothelial cells started to express ICAM-1 and recruited circulating leukocytes [29]. Moreover, also the mechanical strain could induce dangerous inflammatory responses that it would never have been detected in conventional culture models based on static cultures. The detection was quantitated by measuring intracellular production of reactive oxygen species (ROS) using microfluorimetry: the presence of nanoparticles in absence of mechanical stress induced a little or not ROS production, while in presence of physiological levels of cyclic strain (10% at 0.2 Hz), the ROS production increased by more than 4-fold within 2 hours, the presence of the stimulus changes the cells behavior, [29].

Aim of the work

The objective of this study was to develop an alveolus-on-chip system that mimic the structure of the alveolar barrier and the physiological exposure of epithelial cells to air . The system comprises a microfluidic platform made of PDMS, which incorporates a nanofibrous PCL/Gelatin membrane to mimic the basement membrane of the alveolar barrier and a lung fibroblast laden-type I collagen hydrogel to mimic the interstitial space of the alveolar wall. The model utilized in this study involves a co-culture of human alveolar epithelial cells (A549) and human lung fibroblasts (MRC-5) to recreate the complex structure of the thick portion of the alveolar wall. The model was created by initially MRC-5 cells embedded in the collagen hydrogel were seeded on the top side of the electrospun membrane to mimic the interstitium, followed by the addition of A549 cells to simulate the alveolar epithelium. The starting point for the development of this work was the thesis work of Martina Cicolini [55] which design a functional geometry of the PDMS device after a hard work of optimization. The PDMS layers constituting the alveolus-on-chip were obtained from poly(methyl methacrylate) (PMMA) molds, designed through Rhinoceros software and produced by laser ablation technique. In her thesis, the geometry of the microfluidic channels, the shape of the inlets and the number and dimension of the pillars supporting the membrane were optimized after various tests, microfluidic experiments and cell adhesion evaluation. To mimic the composition and the three-dimensional architecture of the human alveolar interstitial space, the collagen hydrogel was formulated following the protocol optimized by Michela Licciardello [56] in her PhD thesis. In her work, the the alveolar-capillary barrier was recreated on an engineered transwell system developed by modifying a transwell insert to accommodate the PCL-Gel membrane. This modification process ensured the preservation of the morphological and physico-chemical composition of the electrospun membrane.

2 Materials and methods

The microfluidic device comprises three PDMS layers. The bottom layer is designed with microfluidic serpentines and a circular culture chamber that includes four pillars to support the PCL/Gelatin membrane that is specifically created for the seeding and maintenance of HULEC-5a cells in its bottom side and collagen hydrogel embedded with MRC-5 fibroblasts on the opposite side. The membrane is held in place, suspended on the culture chamber, between the bottom and top layers. The top layer features a circular hole, exposing the upper part of the membrane to air. The final layer serves as a reservoir and has a larger diameter hole that allows the storage of the A549 epithelial cells' medium until the implementation of the air-liquid interface. Each PDMS layer with its respective pattern was produced using 3D-printed molds. Following the assembly of the layers with the electrospun membrane, endothelial was seeded on the lower side of the membrane, the hydrogel rich in fibroblast was placed on the upper side. Once it reached a solid structure, the epithelial cells were seeded on his upper side.

2.1 3D printing

2.1.1 Mold design

The mold for each layer is designed in the previous work [55] using Rhinoceros software. A CAD model of the mold is created, utilizing a non-uniform rational basis spline (NURBS) mathematical model, which enables the representation of 2D and 3D geometries. The tridimensional model is generated by taking a 2D drawing and extruding each component to form a closed surface. The final CAD design represents the negative of the desired pattern for the PDMS layer. The master for each layer of the device consists of an external frame, measuring 1 mm in thickness and 2 mm in height. This frame serves as a container for the liquid PDMS during the solidification process within the mold. The internal surface of the mold has dimensions of 60 mm x 20 mm.

Figure 30, is specular on the 2 sides with a serpentine, each with a width and height of 600 μm, and it can be accessed through lateral inlet designed in the shape of semi-truncated cones. To enhance the filling process and prevent any leakage from the inlet, the 2 half-inlets of the bottom layer are complemented by their corresponding halves in the top layer. This configuration ensures that the resulting conical shape aligns perfectly with the micropipette tips utilized during the experimental phase. The aim of the 2 serpentines is to maximize the capacity for holding the cell medium, allowing for a larger volume(about 80 μL) to be accommodated and minimizing the need for frequent replenishment during the static phase of the cell culture. To reduce the tendency of liquid to flow back towards the inlet and/or to rise above the membrane in the reservoir instead entering inside the second serpentine, the 2 microfluidic channels are connected to valvular conduits designed on a Nikola Tesla's original patent [57].

The Nikola Tesla's valvular conduit, thanks to its convoluted shapes that

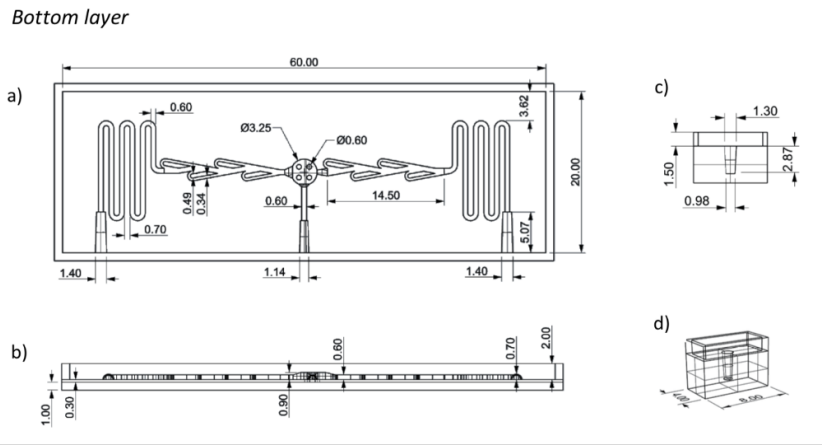

Figure 30: On the left, top view (a) and front view (b) of the CAD model of the master of the bottom layer. On the right, front view (c) and perspective view (d) of the CAD model of the master of the plug for the conic inlets. Dimensions are expressed in millimeters. CAD made via Rhinoceros.

create a preferential path, possesses direction-dependent fluidic resistance [57]. Its purpose is to facilitate the flow of the cell medium in the desired direction (from the left inlet to the right outlet), while preventing the liquid from flowing back or rising above the membrane during the filling of the second turbine. The valvular conduit connects to the central element of the master, which serves as the culture chamber. This circular component, that is the negative of the final PDMS layer, is 1 mm in height and features four holes with a diameter of 600 μm for supporting the PCL/gelatin membrane. Additionally, a smaller central inlet, distinct from the other 2 inlets, provides direct access to the culture chamber through a 600 μm x 600 μm channel. This inlet was specifically used for seeding HULEC-5a cells into the culture chamber. To ensure proper sealing of the central channel when filling the microfluidic channels, a custom mold was created to produce a PDMS plug, as illustrated in Figure 30. This PDMS plug is used to block the central conic inlet in the lower section of the membrane after cell seeding. The plug effectively seals the channel, preventing any leakage or unwanted flow during subsequent steps of the experiment.

In Figure 31, which is 2 mm thick, functions as a seal for the microfluidic channels in the bottom layer. It features three semi-inlets that align with their corresponding counterparts in the lower layer. Its main feature is the central hole of 2 mm height with a diameter of 3.25 mm that exposes the upper part of the membrane to air. It is particularly important for the implementation of the air-liquid interface condition, which is typically required 72 hours after seeding the epithelial cells.

The final layer of the microfluidic device serves as a medium reservoir, Figure 32. For this reason, its main feature is a central hole with an 8 mm diameter and

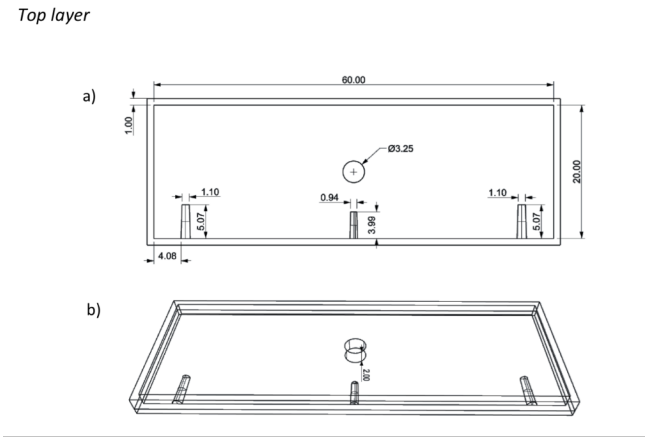

Figure 31: Top view (a) and perspective view (b) of the CAD model of the top layer master. Dimensions are expressed in millimeters. CAD made via Rhinoceros.

2 mm height. It allows for the storage of approximately 100 μl of cell medium. In order to make possible the endothelial cells culture, a plug is designed, Figure 32 c,d. It fits the concentric holes of the top layer and reservoir. The vertical dimensions of the plug are carefully studied to ensure that there is no contact between the plug and the central membrane.

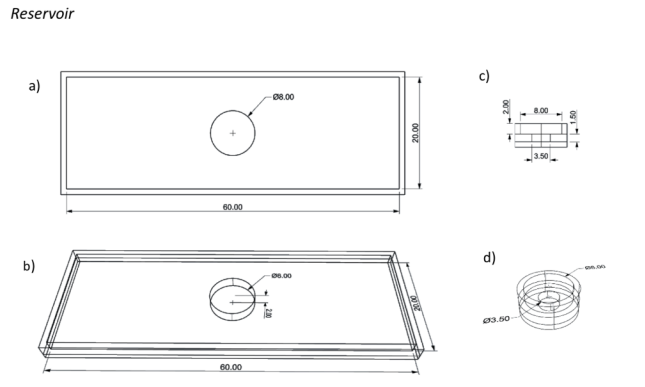

Figure 32: On the left, top view (a) and perspective view (b) of the CAD model of the reservoir master. On the right, front view (c) and perspective view (d) of the CAD model of the master of the plug for the central upper hole. Dimensions are expressed in millimeters. CAD made via Rhinoceros.

2.1.2 Mold fabrication

3D printing is selected as the fabrication technique for the molds due to its favorable throughput/quality ratio. This technique offers several advantages that make it well-suited for the project [58]. Poly-Jet 3D printing, as an additive manufacturing process, operates by sequentially adding layers of a photopolymer resin into a build tray and subsequently curing them using ultraviolet lamps mounted on the 3D printing heads [58]. This technique utilizes a CAD model of the desired geometry as a basis for creating three-dimensional objects. The poly-jet 3D printer used in this work is the OBJET30 Stratasys (Figure 33), characterized by an XY Resolution of 600x600 DPI (dots per inch) and horizontal build layers range between 16 microns and 36 microns depending on the print mode.

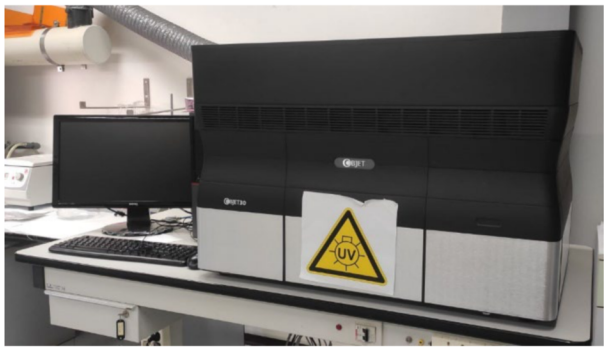

Figure 33: ChiLab OBJET30 Stratasys 3D printer.

The CAD model has to be converted into a STL (Standard Triangulation Language) format and imported to the Objet Studio software of the printer, where the slicing algorithm splits the 3D geometry into two-dimensional slices. After the 3D printing process, the objects are detached from the build tray using a metal spatula. The support material at the base of each piece is then removed and washed off with water. Following this step, the molds undergo a crucial thermal treatment. They are placed into an oven at a temperature of 110°C overnight. This thermal treatment is essential for the successful curing of the PDMS (Polydimethylsiloxane) that will be poured into the 3D printed objects for replica molding. PDMS curing involves the crosslinking of vinyl-terminated oligomers in the presence of a catalyst, typically through a hydrosilylation mechanism. During the curing process, certain molecules with a strong affinity for the catalyst can inhibit the crosslinking reaction. These inhibiting molecules, such as polyethylene glycols, diethyl-phthalates, unreacted monomers, and phosphineoxide photoinitiators, may be released into the solution by the 3D printed objects [59]. The thermal and UV treatments applied to the 3D printed molds have been demonstrated to vaporize the remaining photo-initiators from the

structures and promote recombination reactions between the photo-initiators and any residual high molecular weight species in the resin [59]. These treatments help eliminate any inhibiting molecules and further enhance the curing process, ensuring the production of high-quality PDMS molds.

2.1.3 Replica molding

The replica molding technique is a fast and adaptable method that enables the production of objects. By utilizing the replica molding technique, it becomes possible to achieve high-resolution objects with simplicity, speed, and versatility. The molds can be created using different methods like 3D printing, photolithography, or laser ablation, while the final Young Modulus of the PDMS solution can be adjusted by varying the ratio of the pre-polymer to the reticulating agent. In this study, PDMS replicas are obtained using 3D printed masters, resulting in the creation of elastic and transparent patterned layers.

2.1.4 PDMS layer fabrication

A solution is prepared with a weight ratio of 10:1 (PDMS pre-polymer to reticulating agent) and thoroughly mixed manually. To minimize the occurrence of bubbles, the solution undergoes vacuum degassing process. Following that, the viscous PDMS is meticulously poured into clean molds, ensuring that no meniscus formed. The molds are subsequently placed in an oven set to a temperature of 90°C for a duration of 15 minutes. Once taken out of the oven, the replicas are ready to be peeled off from their molds. After conducting geometry checks and dimensional controls, the layers are immersed in a falcon tube containing ethanol and subjected to a 5-minute ultrasonic bath at a frequency of 49 Hz. To prepare the replicas for plasma oxygen treatment, the cleaned replicas are dried on a hot plate at 80°C for approximately 10 minutes, allowing the surface to be suitably prepared.

2.1.5 PDMS layer characterization

The PDMS layers were characterized by comparing the real dimensions via microscope with the nominal dimensions to evaluate the fidelity. The geometric features chosen are the ones that cells influence. The bottom layer was sectioned to measure the real dimensions of the pillar (height and diameter), the cell chamber (diameter) and the serpentine (diameter and distance), while in the top layer the central hole is measured. The real dimensions were confronted with the nominal dimensions in terms of average and standard deviation.

2.1.6 The Nikola Tesla's characterization

In order to demonstrate how Nikola Tesla's valvular conduit, Figure 34 a, influences the raise of medium over the membrane, the device with 100 μl of a mixture of water and Toluidine Blue to show the difference between devices with and without valvular conduits, Figure 34 b.

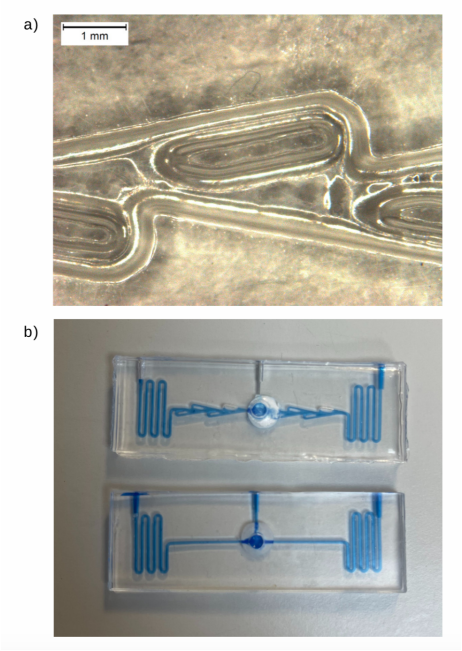

Figure 34: a)Nikola Tesla's valvular conduit b)Comparison beetwen device with and without Nikola Tesla's valvular conduit

2.2 Electrospinning

The alveolar basement membrane was reproduced using the electrospinnig set-up in Figure 35.

Figure 35: Novaspider V5 elettrospinning instrument in PolitoBIOMed Lab.

Electrospinning is a technique for producing fibers by utilizing electric forces to extrude polymeric solutions or melt polymers. The process involves loading a syringe with the desired material and applying a high voltage between the

syringe nozzle and the collector, where the extruded fibers are collected due to the applied voltage. Different types of collectors can be employed based on the intended outcome. Rotating collectors with large diameters are used to obtain aligned fibers, while smaller diameters are useful for creating tubular fibrous scaffolds. In particular, in this wprk, planar collector is utilized, resulting in randomly oriented fibers to mimic the alveolar basement membrane, [60], Figure 36.

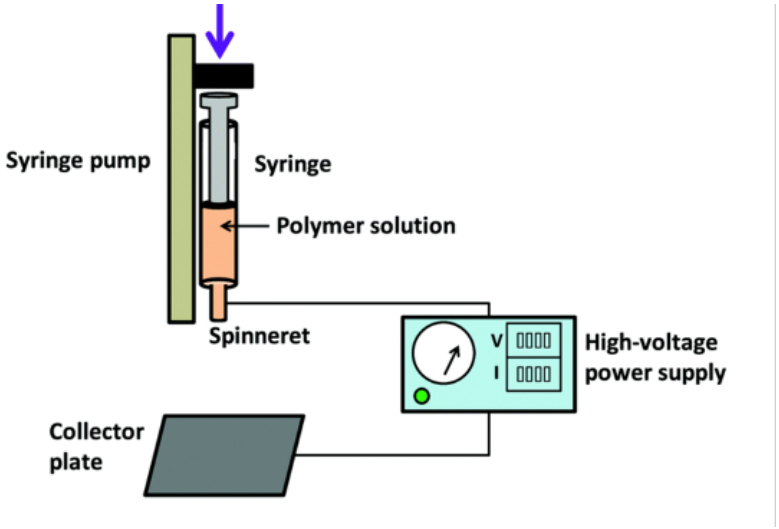

Figure 36: A schematic illustration of the electrospinning process [60].

The electrospinning instrument used to fabricate the membranes is the Novaspider V5 in Figure 35. It allows for movement along the x, y, and z axes while maintaining real-time monitoring and control of the process parameters through an interface accessible via a touch screen panel. The size and quality of the fibers are influenced by several factors, Figure 37. These include the characteristics of the polymeric solutions such as viscosity, surface tension, concentration, molecular weight, and polymer structure. Additionally, the evaporation rate and conductivity of the solvent, as well as the process parameters including voltage, flow rate, and distance between the needle and the collector, play a crucial role. Furthermore, the temperature and humidity of the surrounding environment also impact the final outcome, [61].

Sl. No	Solution Parameters	Effects on Fiber	Mechanism
1	Conductivity of the Solution	It has been demonstrated that increasing the solution conductivity improves the fiber quality, as seen by fewer beads and a smaller fiber diameter.	Increased solution conductivity results in increased stretching of the solution jet due to the solution's larger charge-carrying capacity. Additionally, increasing solution conductivity results in an increase in bending instability and a longer jet path.
	Solution viscosity	Fiber diameter will increase as the viscosity of the fluid increases.	There is a possibility that the charges used to start spinning will not be enough to stretch the solution to reach the target when viscosity increases.
2	Solvent volatility	The location with the greatest solvent volatility must be identified. Ribbon/flat fibers and fibers with surface pores may be produced by using a more volatile solvent.	Wet fibers, fused fibers, or no fiber collection can all occur when a solution is made using a solvent with a low volatility. The solidification of the new polymeric solution at the spinneret tip might cause intermittent spinning when the polymer has a high volatility.
3	Humidity	Larger fiber diameters have been linked to both higher and lower relative humidity levels.	There are two factors that contribute to this: high humidity causes polymer precipitation, preventing fiber elongation; and lower relative humidity causes faster solvent vaporization, which causes an increase in solidification rate that results in larger fiber diameter, thus resulting in thicker fibers.
4	Temperature	The diameter of the fiber will be smaller at higher temperatures.	Higher temperatures result in quicker solvent evaporation and a lower viscosity of the polymer solution.

Figure 37: Influence of solution and process parameters on the morphology of the electrospun fibers [60].

2.2.1 Membrane fabrication and characterization

The chosen material for constructing the alveolus-on-chip scaffold is a blend of PCL (polycaprolactone) and gelatin. This combination involves the integration of a synthetic polymer (PCL, Sigma Aldrich) with a natural polymer (gelatin type A, Sigma Aldrich). In a previous thesis work by Eleonora Palumbo et al. [62], a comparison was made between membranes made solely of PCL and those made of the PCL/gelatin blend. The results indicated that the blend produced fibers and pores with a smaller diameter compared to PCL membranes. However, cyclic uniaxial mechanical tests revealed that incorporating gelatin into the solution enhanced the Young's modulus of the fibers, resulting in a reduction in material elasticity. Overall, the PCL/Gel blend is considered a good compromise between the bioactivity properties of gelatin and the fatigue resistance of PCL. PCL (polycaprolactone) is a semi-crystalline, hydrophobic polyester that is biodegradable. It is synthesized through the ring-opening polymerization of the cyclic monomer ϵ -caprolactone. On the other hand, gelatin is a natural polymer derived from the partial hydrolysis of collagen. The macromolecules of gelatin consist of amino acids such as hydroxyproline, glycine, and proline, which promote cell adhesion, migration, and proliferation. It is important to note that gelatin is water-soluble unless it undergoes crosslinking. The aim is to develop blended scaffolds that combine the benefits of natural and synthetic materials, with the ultimate objective of creating ECM-like structures that possess favorable properties for facilitating the growth of lung cells.

Others test have been done in the previously thesis [56]. In this work [56], there is a comparison between PCL membrane and the combination of PCL/Geltin membrane: the degradation rate of 2 membranes was tested with the FTIR-ATR spectra; the nanofibrous morphology of PCL and PCL-Gel was analyzed by FESEM images and SEM images; the mechanical properties were calculated from the stress-strain curves; the surface wettability was measured with the contact angle. Moreover, the morphology of A549 and HULEC-5a and their viability on PCL and PCL-Gel membranes was evaluated by staining the cell nuclei and actin filaments.

In this work, gelatin was stabilized by crosslinking using (3-Glycidyloxypropyl) trimethoxysilane (GPTMS), a silane coupling agent whose oxirane rings react with the ammino groups of the gelatin, forming pendent silanol groups, Figure 38.

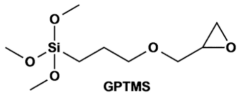

Figure 38: Chemical structure of (3-Glycidyloxypropyl) trimethoxysilane (GPTMS). Image via Wikipedia.

During the fibers extrusion, the solvent evaporates, and Si-O-Si bonds between gelatin macromolecules are formed thanks to condensation reactions of two silanol groups. In this study, a mixture of PCL and gelatin is prepared in an 80:20 weight/weight ratio. This mixture is dissolved in a solution consisting of 5 mL of acetic acid and formic acid in a 50:50 ratio. The resulting solution had a concentration of 15% w/v. To facilitate the polymerization process, a reticulating agent called GPTMS (3.68% v/v) is added to the PCL/gelatin solution after 24 hours of stirring in a glass beaker at room temperature and 200 rpm. The solution is further stirred for an additional 30 minutes and then transferred into a syringe. The extrusion process involved pumping the 5 mL solution at a constant flow rate of 500 μ/min. The distance between the syringe nozzle and the collector is set at 12 cm. A potential difference of 20 kV is applied during electrospinning. These specific parameters were determined based on the optimized combination identified in the previously mentioned work [62].

The morphology of the electrospun fibers was analyzed in the previously work [55] with the scanning electron microscopy (SEM, Tescan Vega) Zeiss SUPRA 40. In this study, SEM was used to evaluate the effects of thermic treatments on the morphology of the fibers of the PCL/Gel membrane.

Scanning Electron Microscopy (SEM) is an advanced imaging technique that offers high-resolution visualization by detecting secondary electrons emitted from the sample when exposed to a focused, high-energy electron beam. The primary electrons necessary for this process are generated using an electron gun and accelerated with a voltage ranging from 1 to 30 kV. A series of electromagnetic lenses then focus the electron beam onto the specimen within a vacuum

chamber. In order to emit secondary electrons, the samples are typically coated with a thin layer of platinum through a process known as sputter-coating before analysis to allow secondary electron emission during SEM imaging.

2.3 Device assembling by plasma treatment

The device assembly involved utilizing plasma treatment. To obtain circular membranes of specific dimensions, the electrospun membrane mats are cut using a 7 mm diameter puncher. Each circular membrane is carefully handled and positioned over the culture chamber on top of a clean PDMS bottom layer. Subsequently, a plasma treatment is conducted at this stage. Plasma oxygen is used to activate the surfaces generating reactive chemical groups for covalent bonding between two PDMS layers. The terminal methyl groups (-CH3) in PDMS (generally comprised of repeating units of – O–Si(CH3)2–), Figure 39, can be replaced by silanol groups (Si-OH).

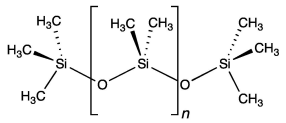

Figure 39: Chemical structure of PDMS. Image via Wikipedia.

The presence of hydroxyl groups allows the irreversible bonding by (Si-O-Si) bonds of the two replicas, after the loss of a water molecule, Figure 40.

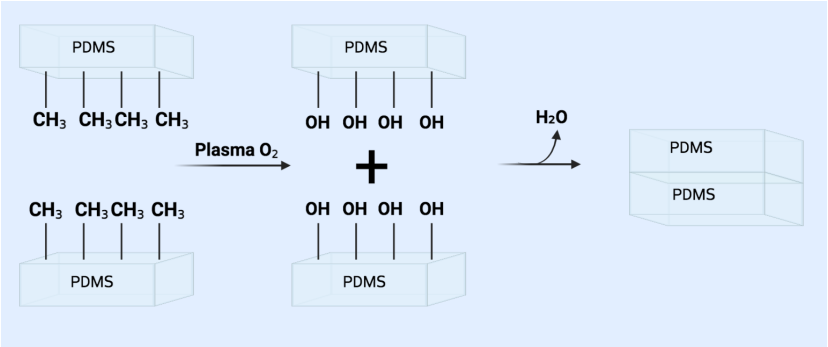

Figure 40: PDMS after Plasma-Oxygen treatment. Image made via Biorender.

The Atto plasma system by Diener electronic (as shown in Figure 41) is utilized for the PDMS activation process, which consists of four phases. These phases are meticulously optimized to achieve the best possible result for PDMS activation.

- Pumping down: once each PDMS replica is positioned in the chamber, with the surface to be functionalized facing upwards, the door is closed.

Figure 41: ChiLab Atto plasma system by Diener electronic.

The subsequent step involves pumping down the chamber, gradually reducing the pressure inside to reach a level of 0.3 mbar.

- Gas supply: oxygen is introduced into the chamber, and the pressure is set to 0.7 mbar. This oxygen pumping process continues for a duration of one minute.
- Plasma process: plasma is produced for 30 seconds.
- Venting: the last phase when the chamber is filled with air and the atmospheric pressure is restored. This phase has a duration of one minute.

  The assembly process involved aligning each layer with its corresponding layer, ensuring that the membrane is properly positioned. In total 2 plasma treatment are done: first one to align the bottom layer with the top and the second one to align the structure bottom/top with the reservoir. For each layer aligning a light pressure is applied to secure the components together. To further enhance adhesion, the assembled structure underwent a thermal treatment on a hot plate. This treatment involved exposing the structure to a temperature of 70°C for a duration of 10 minutes to improve the adhesion between the layers, ensuring a robust and stable assembly.

2.4 Gel formulation and characterization

The hydrogel mimics the structure and composition of the interstitial space and successfully supports the encapsulation of lung fibroblasts, Figure 42.

To mimic the thickest portion of the alveolar wall, type I collagen hydrogel is formulated starting from a 1 % wt./v concentrated solution, to resemble the composition and the three-dimensional architecture of the human alveolar

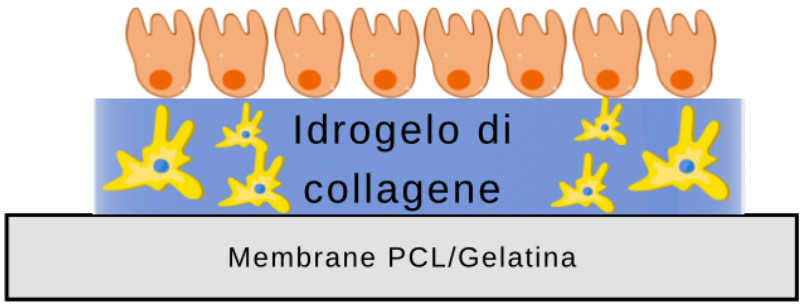

Figure 42: A schematic illustration of the different cell layers. Image made via Biorender.

interstitial space. The hydrogel is combined with MRC-5 fibroblasts and placed over the membrane.

Pre-hydrogel solution is obtained by dispersing gelatin powders in 0.5 M AA in EMEM (AA: Acid Acetic). The suspension is maintained under stirring at 4 °C for 12 hours, obtaining a solution with a hydrogel concentration of 1 % wt./v. The acid pH of the solution is adjusted to approximately 7.5 by adding a 10 M NaOH solution dropwise at 4 °C.

The rheological characterizations were performed in the previously work [56] where the curves of storage modulus (G') and loss modulus (G") were studied. Moreover, swelling and dissolution tests were conducted and to study the biocompatible features of the hydrogel cell viability and proliferation of MRC-5 encapsulated in the hydrogel were evaluated through the metabolic colorimetric assay CellTiter blue (Promega, Italy).

In order to optimize and choose the right volume of hydrogel, once it was colored with Toluidine Blue, 3 volumes of hydrogel 5 μl, 10 μl and 20 μl are placed over the membrane. Once the sol-gel transition is done, devices are sectioned and analyzed via microscope.

2.5 Cell culture

The A549 cells line (adenocarcinomic human alveolar basal epithelial cells) are grown in RPMI 1640 medium (Gibco, ThermoFisher scientific) characterized by the presence of the reducing agent glutathione and high concentrations of vitamins. The RPMI is supplemented with the growth medium that contais several components essential for cell maintenance and vitality. These components included:

- 10% Fetal Bovine Serum (FBS) from Gibco (ThermoFisher Scientific): FBS is a commonly used supplement in cell culture media. It provides essential growth factors, hormones, proteins, and other nutrients necessary for cell growth, maintenance, and vitality.
- 1% L-glutamine 200 nM from Gibco (ThermoFisher Scientific): L-glutamine is an amino acid that plays a crucial role in cell metabolism. It supports the growth of rapidly dividing cells with high energy demands and aids in the synthesis of proteins and nucleic acids. In the case of A549 cells, L-glutamine is particularly important for their specific growth requirements.
- 1% penicillin-streptomycin (P/S) from Gibco (ThermoFisher Scientific): Penicillin and streptomycin are antibiotics commonly added to cell culture media to prevent bacterial contamination. They help maintain a sterile environment for the cells to grow without interference from potential bacterial pathogens. By including 10% FBS, 1% L-glutamine 200 nM, and 1% penicillin-streptomycin in the growth medium, the experiment ensured that the cells received the necessary nutrients, energy support, and protection against bacterial contamination.

The MRC-5 cells are maintained at 37 °C in a humidified atmosphere of 5% CO2 on tissue culture plates (TCP). For biological characterizations, the collagen powders are sterilized with UV light for 30 minutes in ice and acid acetic: EMEM solution are filtered using 0.22 μm filters. In this work, the morphology of MRC-5 fibroblast encapsulated in the hydrogel is investigated by staining cell nuclei and cytoskeletons and with immunostaning of MRC-5 marked by Vimentin. Moreover, live/dead is done to study their viability.

2.5.1 Seeding protocol

To ensure the sterility of each microfluidic chip before seeding, a two-step sterilization process is followed:

1) UV Exposure: Each side of the microfluidic chip is exposed to UV light for a duration of 30 minutes. UV exposure is a common method used to inactivate microorganisms and reduce the risk of contamination.

2) Overnight Incubation with PBS(Phosphate-Buffered Saline), Antibiotic, and Antifungal, a solution to prevent the growth of bacteria and fungi. The sterilizing solution is then removed and the channels are rinsed with PBS.

The starting point of cell seeding was the microfluidic channel filled with cell medium that served as a source of nourishment for the endothelial cells, ensuring their proper growth and function.
After adjusting the solution pH with a sterile NaOH solution, MRC-5 fibroblasts (80-90 % of confluency) are harvested and suspended in pre-hydrogel solution at cell density of 1.5 x 10^6 cells/mL. The solution (10 μL)is plated into the chip (n=4 samples for each condition) and incubated at 37 °C for 30 minutes. Following sol-gel transition, 200 μL of complete medium are added to each chip. The chip is incubated at 37 °C for 30 minutes to promote the sol-gel transition. Then, A549 cells are suspended in MRC-5 cell medium at 1.4 x 10^5 cells/cm^2 and seeded atop the collagen hydrogel.
After 3 days, the medium in the apical chamber is removed and the tri-culture is maintained at ALI for additional 7 days, Figure 43.

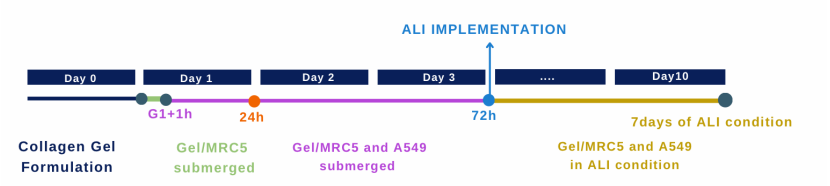

Figure 43: Timeline for the cell seeding co-culture and ALI experiment made via Biorender.

By following this cell seeding and culture protocol, a co-culture system is established within the microfluidic chip, allowing for the study of interactions between MRC-5and A549 cells under ALI conditions to mimic the alveoral barrier.

2.5.2 Fluorescence imaging

DAPI and phalloidin staining, Figure 43, Figure are performed at different time pointing (24h, 72h and 7 days after co-culture seeding) to evaluate the presence of adhered cells and their morphology on the PCL/gel membrane. Here's a breakdown of the protocol:

- Remove the medium from the chip and wash the channels with PBS.
- Fill the channels with 4% paraformaldehyde (PAF) solution. PAF fixates the cells by creating covalent bonds between proteins, making the sample insoluble. The chips are incubated for 30 minutes.
- Wash the samples with PBS to remove the PAF.
- Permeabilize the cellular membranes by treating the samples with 0.5% Triton-X in PBS for 5 minutes. This step allows the staining molecules to enter the cells.

- Wash the samples with PBS for 5 minutes to remove Triton-X.
- Block excess protein-binding sites by incubating the samples with 1% (w/v) bovine serum albumin (BSA) in PBS for 30 minutes. This blocking step helps reduce nonspecific binding of the staining molecules.
- Prepare a solution of 1% BSA and Fluorescein Isothiocyanate Labeled Phalloidin (FITC-phalloidin) in a ratio of 1:60. Phalloidin selectively binds to polymeric F-actin, which is a component of the cytoskeleton. The conjugated FITC provides green fluorescence, allowing the evaluation of cytoskeletal morphology. To achieve this aim, the channels are filled with the phalloidin solution and incubate for 20 minutes in the dark.
- Rinse the samples with PBS for 5 minutes to remove unbound phalloidin.
- Stain the nuclei by preparing a solution of DAPI (diamidino-2-phenylindole) at a concentration of 1:1000 in PBS. DAPI selectively binds to AT sequences of DNA and emits blue fluorescence when bound. Incubate the samples with the DAPI solution for 5 minutes in the dark.
- Wash the samples with PBS for 5 minutes to remove excess DAPI. After following these steps, the samples should be ready for imaging and analysis. The DAPI staining allows visualization of the cell nuclei, while the phalloidin staining provides information about the cytoskeleton morphology and distribution.

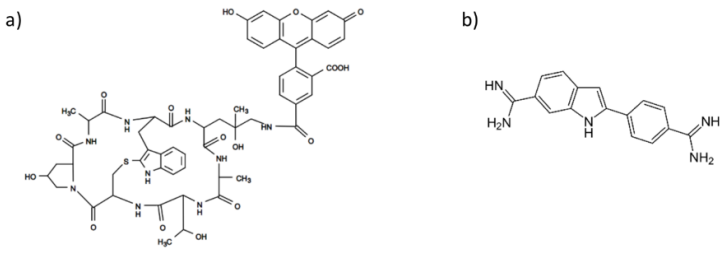

Figure 44: Chemical structure of (a) FITC-phalloidin and (b) DAPI. Chemical structure via Wikipedia.

After disassembling the PDMS devices, the fixed membranes are carefully collected. Each membrane is then sandwiched between two thin glass slides, and a small amount of mounting media (10 μL) for fixed-cell imaging is added to preserve the samples for long-term storage. The slides are properly labeled to indicate the cell type on each side and the fixation time point. To visualize the samples, two imaging systems are employed. First, the Bio-Rad ZOE Fluorescent Cell Imager is used. This instrument utilizes specific wavelengths of light

to isolate fluorophores and capture wide-field fluorescent images. For higher-resolution images, the Nikon Eclipse Ti2 confocal laser scanning microscope is utilized. Images obtained from these imaging systems were then processed and analyzed using software such as ImageJ. By merging images captured in different fluorescent channels, the resulting composite images provided a comprehensive view of the samples' fluorescence signals and cellular structures.

2.5.3 Immunostaining

Immunofluorescence staining is carried out to evaluate the barrier function of the multi-layered model. The objective is to detect the expression of E-cadherin (epithelial cadherin), VE-cadherin which indicates the adherens junctions to mark the alveolar barrier function and Vimentin which selectively stains the presence of fibrob- lasts in the tri-culture model. The immunostaining procedure began with the fixation of cells, which involved washing the samples with PBS and incubating them in 4% PAF for 30 minutes, followed by another PBS wash. Subsequently, permeabi- lization is achieved by treating the samples with 0.2% v/v TRITON-X in PBS for 10 minutes. To prevent non-specific binding, the samples are then blocked using a 2% BSA solution in PBS for an hour. After this step, the samples are ready for overnight incubation at 4°C with primary antibodies dissolved in a solution of PBS, 1% v/v BSA, and 0.1% v/v Tween 20. On the following day, the samples are washed using the same solution. Then, the samples were incubated in a solution of secondary antibodies solution in PBS, 1% v/v BSA, and 0.1

2.5.4 Live/Dead staining

Live/dead staining is carried out to evaluate the rapid quantitation of cell viability using fluorescent microscopy. The Live Dead assay staining solution is a mixture of two fluorescent dyes that differentially label live and dead cells. Live cells are identified on the basis of intracellular esterase activity (generating green fluorescence) and exclusion of the red dye. Dead cells are identified by the lack of esterase activity and non-intact plasma membrane which allows red dye staining: the Live cell dye labels intact, viable cells green and the Dead cell dye labels cells with compromised plasma membranes red. Cells are treated with the following fluorescent solution: 1 mL PBS, 2μl of ethidium to mark in red dead cells and 0.5 μl of calcein to detect in green cells that are alive. Cells are incubated with the solution for 40 minutes and, after, analyzed with the Nikon Eclipse Ti2 confocal laser scanning microscope.

2.5.5 3D reconstruction

The Nikon Eclipse Ti2 confocal laser scanning microscope is utilised in z-stack mode to recreate the thickness of the alveolar barrier. Z-stack is a mathematical reconstruction produce a three-dimensional volume. A set of confocal images taken from the x and y axes creating a 2D image and each 2D slide is stacked

on the other one to build the 3D image along the z axis. Z-stack reconstruction are taken a 7 days after the cell seeding to prove the 3D structur of the alveolar barrier.

3 Results and discussion

Device's characterization

3.1 Dimensional analysis

The PDMS final chip, Figure 45, undergoes characterization by analyzing the disparity between its actual dimensions and the nominal dimensions.

Figure 45: Alveolus-on-a-chip microdevice.

The specific geometric features selected for analysis are those that are most significantly affected by cellular influence, Figure 46.

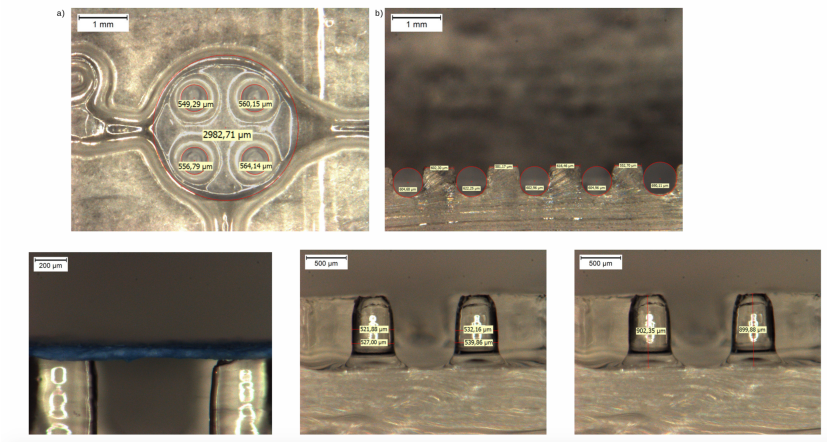

Figure 46: Image of the microfluidic device to analyze real dimensions: a)diameter of chambel cell and pillars b)diameter nd distance of Tesla valvulars c) height of pillars d) width of pillars e)diameter hole of the top layer

To conduct a statistical analysis, 20 different devices are examined, and for each dimension, the average and standard deviation are calculated. This information is provided in the following Figure 47.

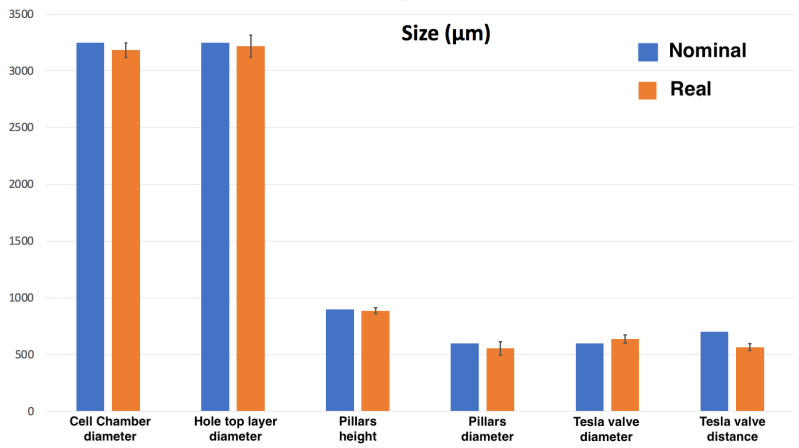

Figure 47: Comparation between nominal and real sizes of n=20 devices.

The difference between the nominal values and the real ones could be due to the nature of the laser ablation technique chosen: molds pattern are some

tens of μm bigger than the CAD model quote, probably due to the small delay between the liquid resin layer deposition and its UV curing and reticulation; moreover, Madsen et al. [63] studied the shrinkage of a PDMS material utilized for measuring nano-metric geometries concluded that the utilized PDMS shrinks linearly between 1% and 3% in the range 40 to 120°C, leading to dimensions that are smaller than the ones of the replicated master.

In conclusion, even if the replica molding has the ability to obtain a replica of the features that are inaccessible for standard measurement devices due to their complex geometry, the PDMS replicas might have geometry dimensions some tens of micrometers different from the nominal ones.

3.2 Gel's characterization

In order to investigate the right gel's volume that could be placed over the membrane, the hydrogel is colored by Touline Blue colorant and different volumes are considered: 5 μl, 10 μl and 20 μl. Once the sol-gel transition is done, the device is sectioned and analyzed via a microscope. Based on the Figure 48, it appears that a favorable balance between the amount of gel used and the sustainability of the membrane is achieved at a volume of 10 μl, which is selected as the gel quantity for the seeding phase.

Following the initial seeding phase, as depicted in the Figure 49, the 10 μl volume of the hydrogel appears to retain its structural integrity through the secretion of a cell matrix by fibroblasts. For this reason, 10 μl was the selected volume.

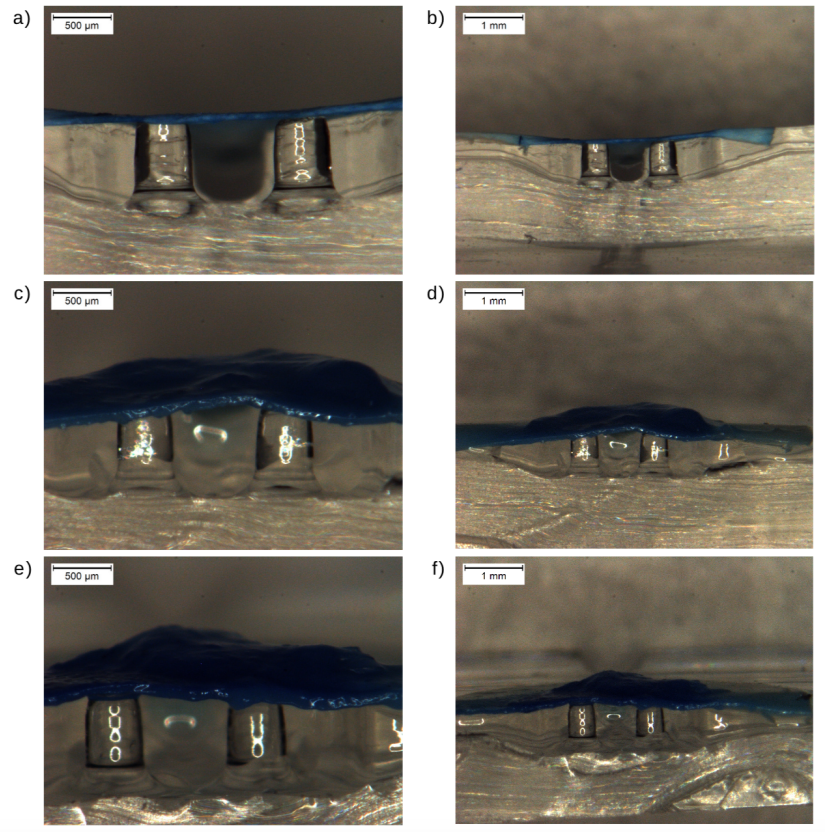

Figure 48: Section of the culture chamber with: a,b) 5 μl of hydrogel volume over the membrane; c,d) 10 μl of hydrogel volume over the membrane; e,f) 20 μl of hydrogel volume over the membrane

Figure 49: Image of the hydrogel (10μl) after the cell experiment.

3.3 The Nikola Tesla's characterization

In order to minimize the liquid's tendency to flow back towards the inlet or rise above the membrane in the reservoir instead of entering the second serpentine, the two microfluidic channels are connected to valvular conduits inspired by Nikola Tesla's original patent. This outcome is examined using an optical microscope, comparing the device with valvular conduits to the device without them (Figure 50 b). As depicted in Figure 50 d, in the device lacking valvular conduits, the liquid rises above the membrane once the conduit is filled with 100 μl of colored water.

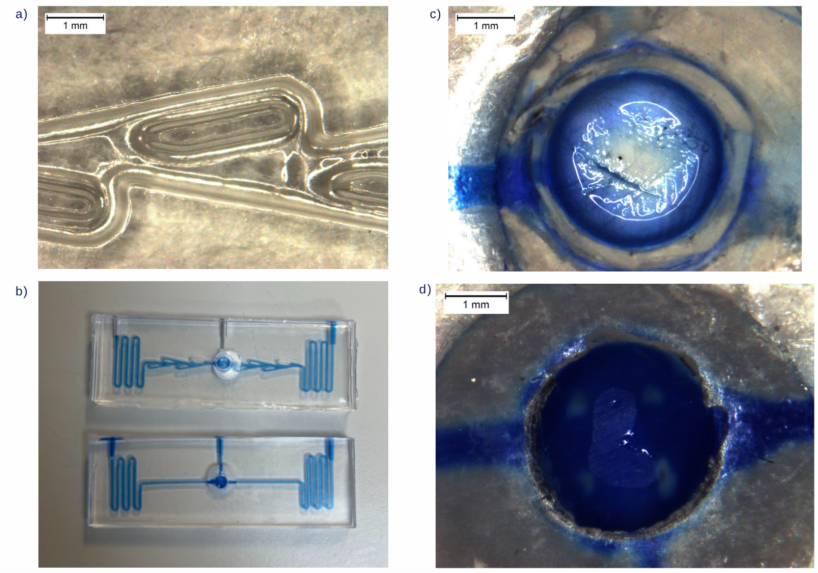

Figure 50: a)Tesla's valvular, b) comparison devise with ant without Tesla's valvular, c)cell chamber device Tesla's valvular, d)cell chamber device without Tesla's valvular

Cellular tests

3.4 Live and dead, immunostaning and fluorescence staining

To demonstrate the ability of the device to sustain the recreation of the alveolar barrier, a cell viability analysis was conducted 24 hours after seeding to determine the percentage of live and dead cells. As depicted in Figure 51, it was observed that all cells remained viable after 24 hours. This time pointing was chosen to demostrate how the device was capable to reproduce a safe environment for the cell seeding and growthing. The analysis after 24h from the starting of experiment is the most selected choise, as in this review [64] where live/dead essay was carried out to evaluate, inside a lung-on-a-chip model, the pH-responsive off HSA-ZnO nanoparticles after 24 hourd from the seeding.

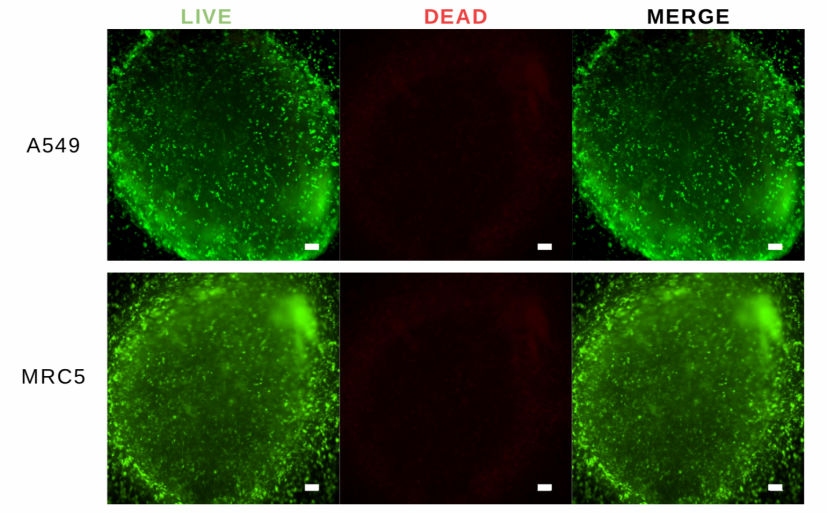

Figure 51: Confocal cell Live(green) and Dead(red) images after 24h, scale bar 20μm.

In order to evaluate the cells morphology of the alveolar barrier and its confluence, once the multi-cellular culture is seeded, DAPI and Phalloidin staining is done a 72 hours. The multi-culture is performed for 3 days under liquid-liquid interface condition. The staining of cell nuclei and F-actin filaments, Figure 52 , demonstrated that uniform epithelial layers of cells is obtained after 3 days of culture.

Once the confluence is obtained, ALI is achieved by removing the medium from the top side of the alveolus-on-chip and continuing the cell culture for an additional 7 days. In order to validate the Air liquide interface, epithelial cells morphology are analyzed by DAPI, phalloidin and E-cadherin (epithelial cadherin).

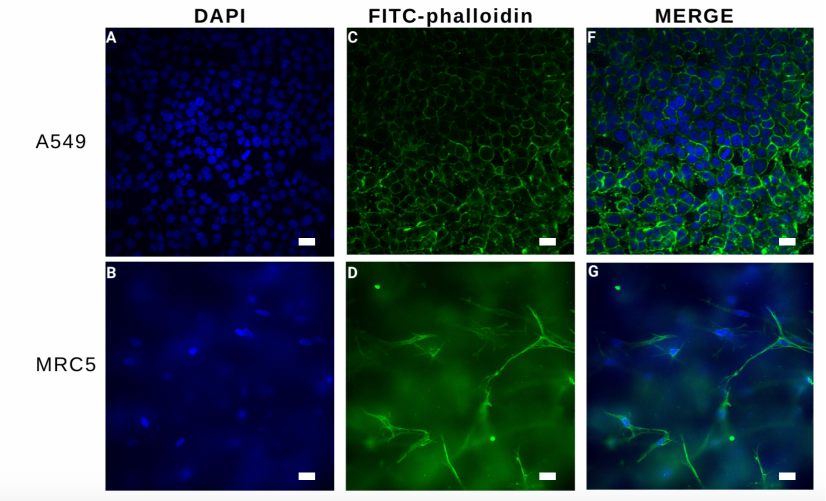

Figure 52: Confocal laser scanning images after fixation and staining at 72h with DAPI (A,B) and phalloidin (C,D) and their merge (E,F), scale bar 20μm.

After 7 days of co-culture at the air-liquid interface (ALI), confocal laser scanning images Figure 53 and 54 in C images demonstrate the expression of E-cadherins, which are involved in the formation of adherens junctions, in A549 cells. The localization of E-cadherins is observed along the cell membrane, specifically between neighboring cells. The epithelial morphology is also dimostrated by phalloidin and DAPI confocal images, in both merged images. Immunofluorescence staining of cells confirmed that confluent layers of cells were obtained for A549 ephitelial cells.

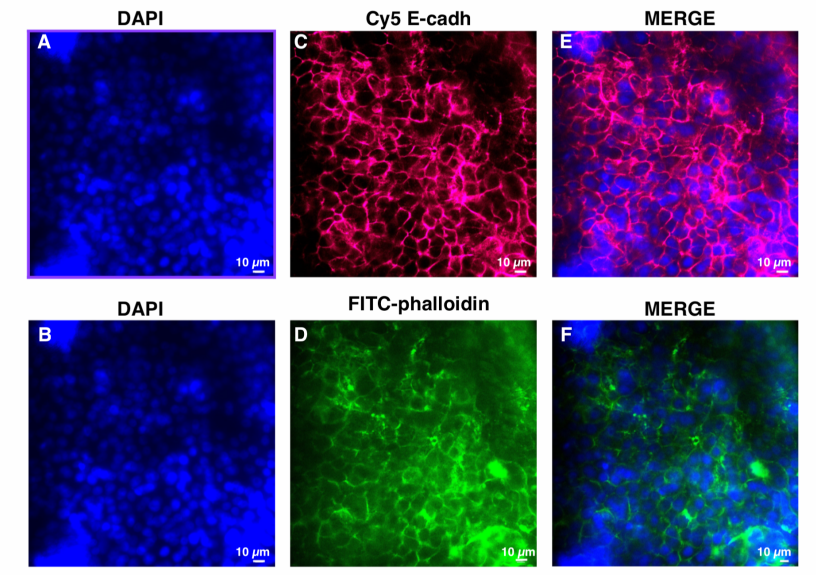

Figure 53: Immunofluorescence staining of the A549 cells for DAPI (A,B), Cy5-Ecadh (C), FITC.phalloidin (D) and their merge (E,F), scale bar 10 μm.

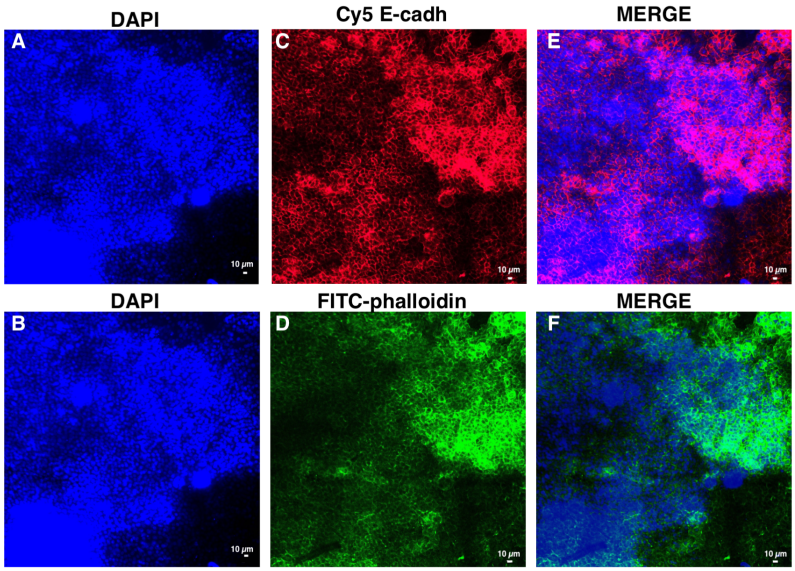

Figure 54: Images after fixation and staining of A549 cells for DAPI (A,B), Cy5-Ecadh (C), FITC.phalloidin (D) and their merge (E,F), scale bar 10μm.

To assess the morphology of MRC-5 cells encapsulated in the hydrogel, staining of the cell nuclei and actin filaments was performed. As shown in the Figure 55 fibroblasts appeared uniformly distributed within the volume of the hydrogel.

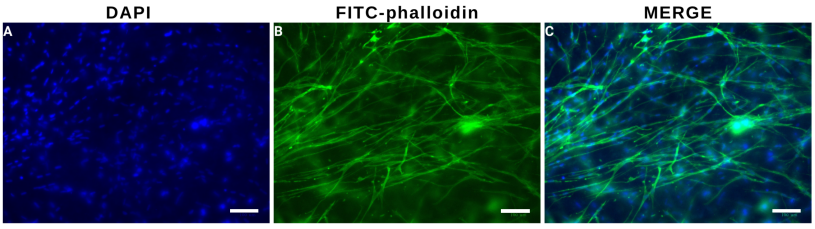

Figure 55: Images after fixation and staining of MRC-5 cells at 7 days with DAPI (A) and phalloidin (B) and their merge (C), scale bar 100μm.

In addition, MRC-5 cells were examined using immunostaining for Vimentin, an intermediate filament protein expressed in fibroblasts. In Figure 56, the MRC-5 fibroblasts exhibit their characteristic elongated and spindle-like morphology, as indicated by the staining of Vimentin.

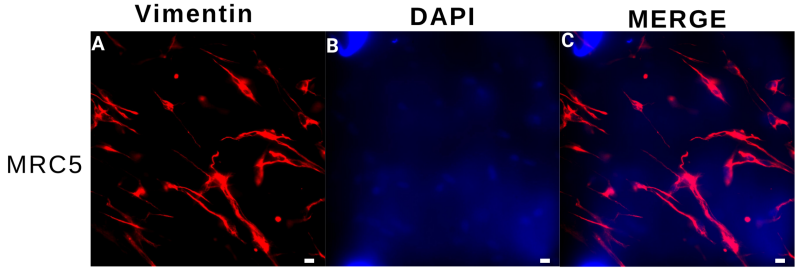

Figure 56: Immunofluorescence staining of MRC-5 cells at 7 days with Vimentin (A) and DAPI (B) and their merge (C), scale bar 10μm.

Moreover, the Figure 57 shows Vimentin marks of a bigger hydrogel's portion to emphasize the MRC-5 fibroblasts confluence and morphology.

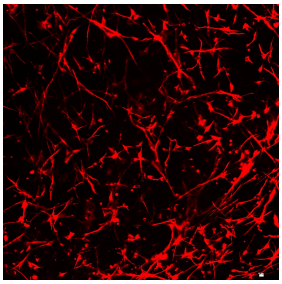

Figure 57: Immunofluorescence staining of Vimentin in MRC-5 cells at 7 days, scale bar 10μm.

After 7 days of cuture in ALI condition, the cell viability was analyzed and, as shown in Figure 58, the quantity of dead cells is notably smaller in comparison to the live cells, emphasizing that the alveolus-on-chip was successfully well projected to sustain cell viability even after 7 days without cell medium. This observation underscores the capability of the chip to effectively support and maintain the vitality of the cells over an extended period of time.

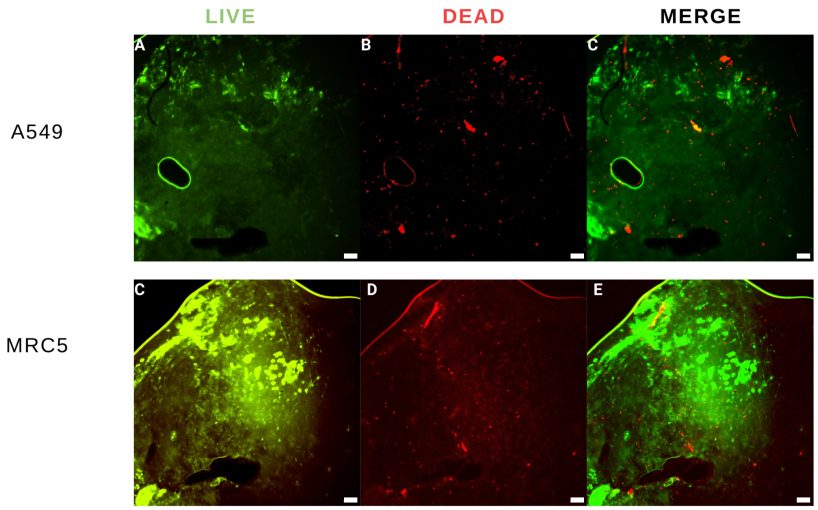

Figure 58: Confocal cell Live(green) and Dead(red) images after 7 days, scale bar 100μm.

In order to validate the ALI condition, numerous studies have documented the capacity of lung epithelial cells to undergo polarization when exposed to air under normal physiological conditions, for example in this work [65] where, to provide physiologically more representative exposure conditions and increase

the differentiation state, Calu-3 bronchial epithelial cells are cultured at an air-liquid interface (ALI) and show their phenotype upon culture in ALI. Moreover, also Kreft, Mateja Erdani, et al. [66] have shown how the Air liquide interface resulted in a more biomimetic native bronchial epithelium displaying pseudostratified columnar epithelium with more microvilli and secretory vesicles during the characterization of the human cell line Calu-3.

3.5 3D reconstruction

3D reconstruction via z-stack was used to analyze the 3 dimentionality of the alveolar barrier. Figure 59 shows the successful achievement of a complete 3D reconstruction through various perspectives after 7 days of air-liquid interface (ALI) culture. The hydrogel, embedded with healthy fibroblasts, displays excellent morphology, while the epithelial cells exhibit a high level of confluence over the hydrogel. This result demonstrates the successful integration and growth of both cell types within the hydrogel.

At present, the hydrogel embedding technique employed for constructing the three-dimensional alveolar stroma encounters difficulties in producing a hydrogel that closely resembles the thickness of human tissues. Nevertheless, by incorporating additional cellular components of the alveolar environment like fibroblasts, it may be feasible to further recreate the thickness of the alveolar stroma, as shown in this thesis as well as in the Varone, Antonio, et al. [67] Alveolus-Chip.

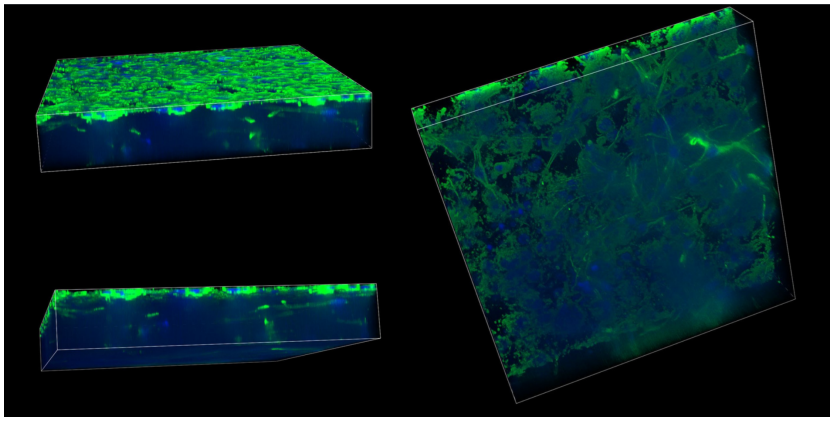

Figure 59: 3D reconstruction of DAPI-phalloidin stained of both MRC-5 fibroblasts encapsulated in hydrogel and A549 cells at 7 days of ALI.

References

[1] Lars Knudsen and Matthias Ochs. The micromechanics of lung alveoli: structure and function of surfactant and tissue components. *Histochemistry and cell biology*, 150:661–676, 2018.

[2] Johan Petersson and Robb W Glenny. Gas exchange and ventilation–perfusion relationships in the lung. *European Respiratory Journal*, 44(4):1023–1041, 2014.

[3] Apeksh Patwa and Amit Shah. Anatomy and physiology of respiratory system relevant to anaesthesia. *Indian journal of anaesthesia*, 59(9):533–541, 2015.

[4] Connie CW Hsia, Dallas M Hyde, and Ewald R Weibel. Lung structure and the intrinsic challenges of gas exchange. *Comprehensive physiology*, 6(2):827, 2016.

[5] Alyssa J Miller and Jason R Spence. In vitro models to study human lung development, disease and homeostasis. *Physiology*, 32(3):246–260, 2017.

[6] Connie CW Hsia, Dallas M Hyde, and Ewald R Weibel. Lung structure and the intrinsic challenges of gas exchange. *Comprehensive physiology*, 6(2):827, 2016.

[7] Johan Petersson and Robb W Glenny. Gas exchange and ventilation–perfusion relationships in the lung. *European Respiratory Journal*, 44(4):1023–1041, 2014.

[8] Loïc Guillot, Nadia Nathan, Olivier Tabary, Guillaume Thouvenin, Philippe Le Rouzic, Harriet Corvol, Serge Amselem, and Annick Clement. Alveolar epithelial cells: master regulators of lung homeostasis. *The international journal of biochemistry & cell biology*, 45(11):2568–2573, 2013.

[9] Xianxian Jia, Bo Wu, Jinhui Huang, Lin Fan, Miao Yang, and Wei Xu. Yap and wnt3a independently promote aeciis proliferation and differentiation by increasing nuclear β-catenin expression in experimental bronchopulmonary dysplasia. *International Journal of Molecular Medicine*, 47(1):195–206, 2021.

[10] Dan Li, Xianzheng Wang, Yingzhao Liao, Shouchuan Wang, Jinjun Shan, and Jianjian Ji. Insights gained into the treatment of covid19 by pulmonary surfactant and its components. *Frontiers in Immunology*, page 2078, 2022.

[11] Ali Doryab, Sinem Tas, Mehmet Berat Taskin, Lin Yang, Anne Hilgendorff, Jürgen Groll, Darcy E Wagner, and Otmar Schmid. Evolution of bioengineered lung models: recent advances and challenges in tissue mimicry for studying the role of mechanical forces in cell biology. *Advanced functional materials*, 29(39):1903114, 2019.

[12] RC Geiger, W Taylor, MR Glucksberg, and DA Dean. Cyclic stretch-induced reorganization of the cytoskeleton and its role in enhanced gene transfer. *Gene therapy*, 13(8):725–731, 2006.

[13] Nicholas E Vlahakis, Mark A Schroeder, Andrew H Limper, and Rolf D Hubmayr. Stretch induces cytokine release by alveolar epithelial cells in vitro. *American Journal of Physiology-Lung Cellular and Molecular Physiology*, 277(1):L167–L173, 1999.

[14] Lynn M Crosby and Christopher M Waters. Epithelial repair mechanisms in the lung. *American Journal of Physiology-Lung Cellular and Molecular Physiology*, 298(6):L715–L731, 2010.

[15] Zuzana Nova, Henrieta Skovierova, and Andrea Calkovska. Alveolar-capillary membrane-related pulmonary cells as a target in endotoxin-induced acute lung injury. *International Journal of Molecular Sciences*, 20(4):831, 2019.

[16] Paul W Noble, Christina E Barkauskas, Dianhua Jiang, et al. Pulmonary fibrosis: patterns and perpetrators. *The Journal of clinical investigation*, 122(8):2756–2762, 2012.

[17] Srikanth Karnati, Michael Seimetz, Florian Kleefeldt, Avinash Sonawane, Thati Madhusudhan, Akash Bachhuka, Djuro Kosanovic, Norbert Weissmann, Karsten Krüger, and Süleyman Ergün. Chronic obstructive pulmonary disease and the cardiovascular system: vascular repair and regeneration as a therapeutic target. *Frontiers in Cardiovascular Medicine*, 8:649512, 2021.

[18] Michael A Matthay, Rachel L Zemans, Guy A Zimmerman, Yaseen M Arabi, Jeremy R Beitler, Alain Mercat, Margaret Herridge, Adrienne G Randolph, and Carolyn S Calfee. Acute respiratory distress syndrome. *Nature reviews Disease primers*, 5(1):18, 2019.

[19] David M Smadja, Steven J Mentzer, Michaela Fontenay, Mike A Laffan, Maximilian Ackermann, Julie Helms, Danny Jonigk, Richard Chocron, Gerald B Pier, Nicolas Gendron, et al. Covid-19 is a systemic vascular hemopathy: insight for mechanistic and clinical aspects. *Angiogenesis*, 24:755–788, 2021.

[20] P Mukherjee, S Roy, D Ghosh, and SK Nandi. Role of animal models in biomedical research: a review. *Laboratory Animal Research*, 38(1):18, 2022.

[21] A Abdullahi, S Amini-Nik, and MG Jeschke. Animal models in burn research. *Cellular and molecular life sciences*, 71:3241–3255, 2014.

[22] Nathan J Weyand. Neisseria models of infection and persistence in the upper respiratory tract. *Pathogens and disease*, 75(3):ftx031, 2017.

[23] Raquel Sanchez-Varo, Marina Mejias-Ortega, Juan Jose Fernandez-Valenzuela, Cristina Nuñez-Diaz, Laura Caceres-Palomo, Laura Vegas-Gomez, Elisabeth Sanchez-Mejias, Laura Trujillo-Estrada, Juan Antonio Garcia-Leon, Ines Moreno-Gonzalez, et al. Transgenic mouse models of alzheimer's disease: An integrative analysis. *International Journal of Molecular Sciences*, 23(10):5404, 2022.

[24] Brigid LM Hogan, Christina E Barkauskas, Harold A Chapman, Jonathan A Epstein, Rajan Jain, Connie CW Hsia, Laura Niklason, Elizabeth Calle, Andrew Le, Scott H Randell, et al. Repair and regeneration of the respiratory system: complexity, plasticity, and mechanisms of lung stem cell function. *Cell stem cell*, 15(2):123–138, 2014.

[25] Konstantinos Gkatzis, Sara Taghizadeh, Dongeun Huh, Didier YR Stainier, and Saverio Bellusci. Use of three-dimensional organoids and lung-on-a-chip methods to study lung development, regeneration and disease. *European Respiratory Journal*, 52(5), 2018.

[26] Kim Charles Aske and Courtney Alice Waugh. Expanding the 3r principles: more rigour and transparency in research using animals. *EMBO reports*, 18(9):1490–1492, 2017.

[27] Lucas B Edelman, James A Eddy, and Nathan D Price. In silico models of cancer. *Wiley Interdisciplinary Reviews: Systems Biology and Medicine*, 2(4):438–459, 2010.

[28] Myrianthi Hadjicharalambous, Peter A Wijeratne, and Vasileios Vavourakis. From tumour perfusion to drug delivery and clinical translation of in silico cancer models. *Methods*, 185:82–93, 2021.

[29] Rafael Agujetas, Raúl Barrio-Perotti, Conrado Ferrera, Adrián Pandal-Blanco, D Keith Walters, and Ana Fernández-Tena. Construction of a hybrid lung model by combining a real geometry of the upper airways and an idealized geometry of the lower airways. *Computer Methods and Programs in Biomedicine*, 196:105613, 2020.

[30] Yoshinori Imamura, Toru Mukohara, Yohei Shimono, Yohei Funakoshi, Naoko Chayahara, Masanori Toyoda, Naomi Kiyota, Shintaro Takao, Seishi Kono, Tetsuya Nakatsura, et al. Comparison of 2d-and 3d-culture models as drug-testing platforms in breast cancer. *Oncology reports*, 33(4):1837–1843, 2015.

[31] Natalie Heinen, Mara Klöhn, Eike Steinmann, and Stephanie Pfaender. In vitro lung models and their application to study sars-cov-2 pathogenesis and disease. *Viruses*, 13(5):792, 2021.

[32] Anke-Gabriele Lenz, Erwin Karg, Ellen Brendel, Helga Hinze-Heyn, Konrad L Maier, Oliver Eickelberg, Tobias Stoeger, and Otmar Schmid. Inflammatory and oxidative stress responses of an alveolar epithelial cell line

to airborne zinc oxide nanoparticles at the air-liquid interface: a comparison with conventional, submerged cell-culture conditions. *BioMed research international*, 2013, 2013.

[33] A Holownia, P Wielgat, A Kwolek, K Jackowski, and JJ Braszko. Crosstalk between co-cultured a549 cells and thp1 cells exposed to cigarette smoke. *Pulmonary Function*, pages 47–55, 2015.

[34] Thijs Pasman, Danielle Baptista, Sander van Riet, Roman K Truckenmüller, Pieter S Hiemstra, Robbert J Rottier, Naomi M Hamelmann, Jos MJ Paulusse, Dimitrios Stamatialis, and André A Poot. Development of an in vitro airway epithelial–endothelial cell culture model on a flexible porous poly (trimethylene carbonate) membrane based on calu-3 airway epithelial cells and lung microvascular endothelial cells. *Membranes*, 11(3):197, 2021.

[35] M Heller, EV Frerick-Ochs, H-K Bauer, E Schiegnitz, D Flesch, J Brieger, R Stein, B Al-Nawas, C Brochhausen, JW Thüroff, et al. Tissue engineered pre-vascularized buccal mucosa equivalents utilizing a primary triculture of epithelial cells, endothelial cells and fibroblasts. *Biomaterials*, 77:207–215, 2016.

[36] François Bertaux, Sebastián Sosa-Carrillo, Viktoriia Gross, Achille Fraisse, Chetan Aditya, Mariela Furstenheim, and Gregory Batt. Enhancing bioreactor arrays for automated measurements and reactive control with reacsight. *Nature Communications*, 13(1):3363, 2022.

[37] Thomas H Petersen, Elizabeth A Calle, Maegen B Colehour, and Laura E Niklason. Bioreactor for the long-term culture of lung tissue. *Cell transplantation*, 20(7):1117–1126, 2011.

[38] Andrew P Price, Kristen A England, Amy M Matson, Bruce R Blazar, and Angela Panoskaltsis-Mortari. Development of a decellularized lung bioreactor system for bioengineering the lung: the matrix reloaded. *Tissue engineering Part A*, 16(8):2581–2591, 2010.

[39] Aleksander Skardal, Sean V Murphy, Mahesh Devarasetty, Ivy Mead, Hyun-Wook Kang, Young-Joon Seol, Yu Shrike Zhang, Su-Ryon Shin, Liang Zhao, Julio Aleman, et al. Multi-tissue interactions in an integrated three-tissue organ-on-a-chip platform. *Scientific reports*, 7(1):8837, 2017.

[40] Ghazaleh Gharib, İsmail Bütün, Zülâl Muganlı, Gül Kozalak, İlayda Namlı, Seyedali Seyedmirzaei Sarraf, Vahid Ebrahimpour Ahmadi, Erçil Toyran, Andre J van Wijnen, and Ali Koşar. Biomedical applications of microfluidic devices: A review. *Biosensors*, 12(11):1023, 2022.

[41] Sagar Regmi, Chetan Poudel, Rameshwar Adhikari, and Kathy Qian Luo. Applications of microfluidics and organ-on-a-chip in cancer research. *Biosensors*, 12(7):459, 2022.

[42] Lin Lin and Chen-Kuei Chung. Pdms microfabrication and design for microfluidics and sustainable energy application. *Micromachines*, 12(11):1350, 2021.

[43] Inês Miranda, Andrews Souza, Paulo Sousa, João Ribeiro, Elisabete MS Castanheira, Rui Lima, and Graça Minas. Properties and applications of pdms for biomedical engineering: A review. *Journal of Functional Biomaterials*, 13(1):2, 2021.

[44] Mika Salmi. Additive manufacturing processes in medical applications. *Materials*, 14(1):191, 2021.

[45] Szymon Baczyński, Piotr Sobotka, Kasper Marchlewicz, Mateusz Słowikowski, Marcin Juchniewicz, Artur Dybko, and Katarzyna A Rutkowska. Orientation of liquid crystalline molecules on pdms surfaces and within pdms microfluidic systems. *Applied Sciences*, 11(24):11593, 2021.

[46] Chao Ma, Yansong Peng, Hongtong Li, and Weiqiang Chen. Organ-on-a-chip: a new paradigm for drug development. *Trends in pharmacological sciences*, 42(2):119–133, 2021.

[47] Tanya J Bennet, Avineet Randhawa, Jessica Hua, and Karen C Cheung. Airway-on-a-chip: designs and applications for lung repair and disease. *Cells*, 10(7):1602, 2021.

[48] Yaqiong Guo, Ronghua Luo, Yaqing Wang, Pengwei Deng, Tianzhang Song, Min Zhang, Peng Wang, Xu Zhang, Kangli Cui, Tingting Tao, et al. Sars-cov-2 induced intestinal responses with a biomimetic human gut-on-chip. *Science bulletin*, 66(8):783–793, 2021.

[49] Min Zhang, Peng Wang, Ronghua Luo, Yaqing Wang, Zhongyu Li, Yaqiong Guo, Yulin Yao, Minghua Li, Tingting Tao, Wenwen Chen, et al. Biomimetic human disease model of sars-cov-2-induced lung injury and immune responses on organ chip system. *Advanced Science*, 8(3):2002928, 2021.

[50] Haiqing Bai, Longlong Si, Amanda Jiang, Chaitra Belgur, Yunhao Zhai, Roberto Plebani, Crystal Yuri Oh, Melissa Rodas, Aditya Patil, Atiq Nurani, et al. Mechanical control of innate immune responses against viral infection revealed in a human lung alveolus chip. *Nature Communications*, 13(1):1928, 2022.

[51] Milad Radiom, Yong He, Juan Peng-Wang, Armelle Baeza-Squiban, Jean-François Berret, and Yong Chen. Alveolar mimics with periodic strain and its effect on the cell layer formation. *Biotechnology and Bioengineering*, 117(9):2827–2841, 2020.

[52] A Jain, R Barrile, AD van der Meer, A Mammoto, T Mammoto, K De Ceunynck, and O Aisiku. 721 otieno, ma, louden, cs, hamilton, ga et al.(2018) primary human lung alveolus-on-a-chip 722 model of intravascular thrombosis for assessment of therapeutics. *Clin Pharmacol Ther*, 103(723):332–340.

[53] Ting Cao, Changmin Shao, Xiaoyu Yu, Ruipei Xie, Chen Yang, Yulong Sun, Shaohua Yang, Wangjian He, Ye Xu, Qihui Fan, et al. Biomimetic alveolus-on-a-chip for sars-cov-2 infection recapitulation. *Research*, 2022.

[54] Dongeun Huh, Benjamin D Matthews, Akiko Mammoto, Martín Montoya-Zavala, Hong Yuan Hsin, and Donald E Ingber. Reconstituting organ-level lung functions on a chip. *Science*, 328(5986):1662–1668, 2010.

[55] Cicolini Martina. Development of a microfluidic alveolus-on-chip supporting epithelial-endothelial cells co-culture and air-liquid interface implementation for the modelling of the physiological alveolar-capillary barrier. *Master Degree Thesis, Politecnico di Torino*, 2022.

[56] Licciardello Michela. Engineered in vitro models to mimic the anatomy and physiology of the human alveolus through advanced biomaterials and nanotechnologies. *Doctoral Degree Thesis, Politecnico di Torino*, 2022.

[57] S Zhang, SH Winoto, and HT Low. Performance simulations of tesla microfluidic valves. In *International Conference on Integration and Commercialization of Micro and Nanosystems*, volume 42657, pages 15–19, 2007.

[58] M Attaran. Sciencedirect the rise of 3-d printing: The advantages of additive manufacturing over traditional manufacturing. *Bus. Horiz., no*, 2017.

[59] Bastien Venzac, Shanliang Deng, Ziad Mahmoud, Aufried Lenferink, Aurélie Costa, Fabrice Bray, Cees Otto, Christian Rolando, and Séverine Le Gac. Pdms curing inhibition on 3d-printed molds: why? also, how to avoid it? *Analytical chemistry*, 93(19):7180–7187, 2021.

[60] Karolina Dziemidowicz, Qingqing Sang, Jinglei Wu, Ziwei Zhang, Fenglei Zhou, Jose M Lagaron, Xiumei Mo, Geoff JM Parker, Deng-Guang Yu, Li-Min Zhu, et al. Electrospinning for healthcare: Recent advancements. *Journal of Materials Chemistry B*, 9(4):939–951, 2021.

[61] Balaji Ayyanar Chinnappan, Marimuthu Krishnaswamy, Huaizhong Xu, and Md Enamul Hoque. Electrospinning of biomedical nanofibers/nanomembranes: effects of process parameters. *Polymers*, 14(18):3719, 2022.

[62] Palumbo Eleonora. The alveolus-on-a-chip: a biomimetic, microfluidic in vitro model of the alveolar-capillary barrier. *Master Degree Thesis, Politecnico di Torino*, 2021.

[63] Morten Hannibal Madsen, Nikolaj A Feidenhans, Poul-Erik Hansen, Jørgen Garnæs, and Kai Dirscherl. Accounting for pdms shrinkage when replicating structures. *Journal of Micromechanics and Microengineering*, 24(12):127002, 2014.

[64] Nileshkumar Meghani, Kyung Hwan Kim, Soo Hwan Kim, Sang Ho Lee, and Kyung Hyun Choi. Evaluation and live monitoring of ph-responsive hsa-zno nanoparticles using a lung-on-a-chip model. *Archives of Pharmacal Research*, 43:503–513, 2020.

[65] Kristin Öhlinger, Tatjana Kolesnik, Claudia Meindl, Birgit Gallé, Markus Absenger-Novak, Dagmar Kolb-Lenz, and Eleonore Fröhlich. Air-liquid interface culture changes surface properties of a549 cells. *Toxicology in Vitro*, 60:369–382, 2019.

[66] Mateja Erdani Kreft, Urška Dragin Jerman, Eva Lasič, Neli Hevir-Kene, Tea Lanišnik Rižner, Luka Peternel, and Katja Kristan. The characterization of the human cell line calu-3 under different culture conditions and its use as an optimized in vitro model to investigate bronchial epithelial function. *European Journal of Pharmaceutical Sciences*, 69:1–9, 2015.

[67] Antonio Varone, Justin Ke Nguyen, Lian Leng, Riccardo Barrile, Josiah Sliz, Carolina Lucchesi, Norman Wen, Achille Gravanis, Geraldine A Hamilton, Katia Karalis, et al. A novel organ-chip system emulates three-dimensional architecture of the human epithelia and the mechanical forces acting on it. *Biomaterials*, 275:120957, 2021.